Volume 14 | Number 6 | June 2017

www.plasma-polymers.org

PLASMA PROCESSES AND POLYMERS

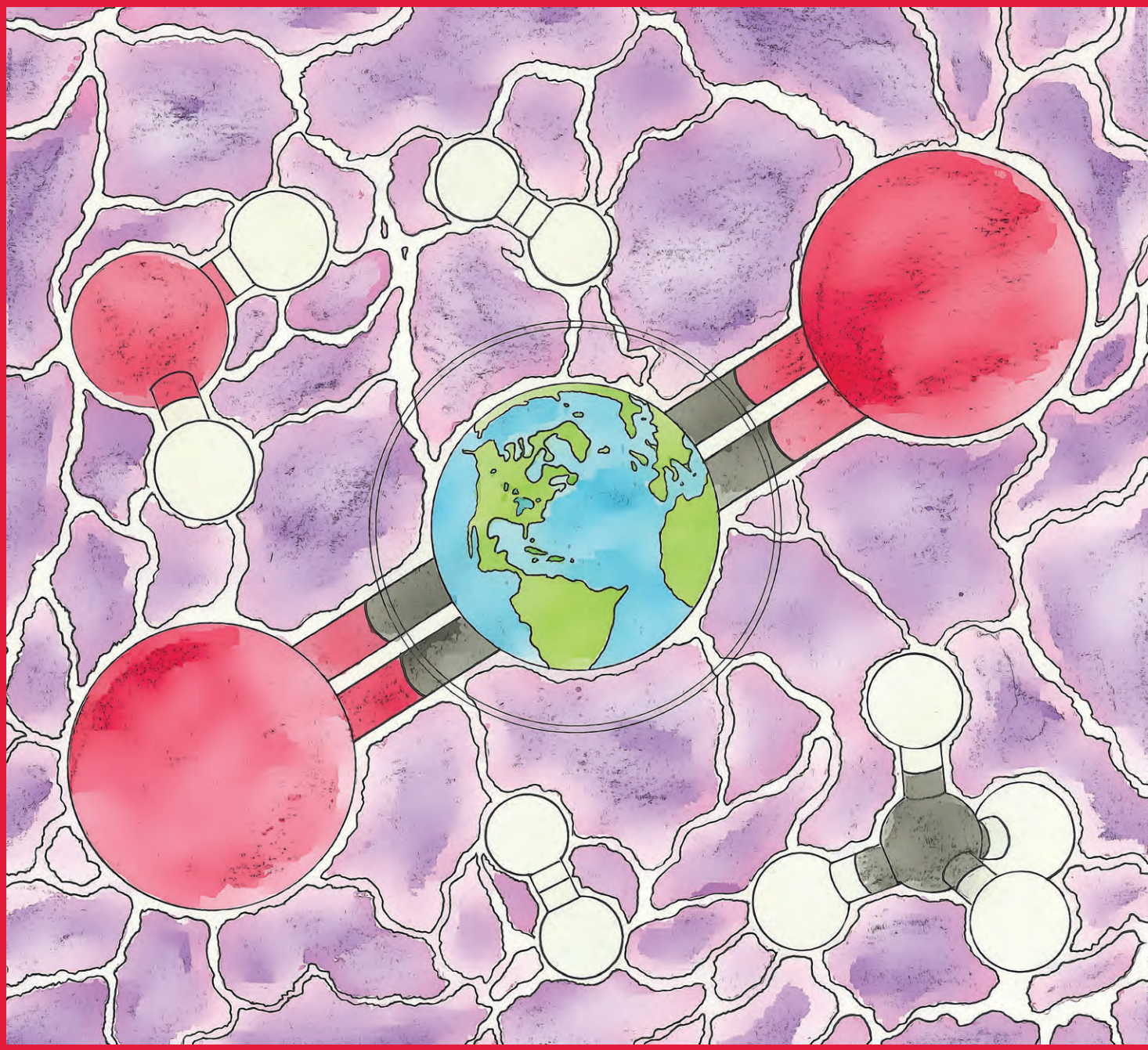

Special Issue:
Plasma Conversion

Guest Editors:
Tomohiro Nozaki | Annemie Bogaerts | Xin Tu | Richard van de Sanden

WILEY-VCH

Received: 19 May 2016 | Revised: 26 August 2016 | Accepted: 26 August 2016

DOI 10.1002/ppap.201600070

PLASMA PROCESSES AND POLYMERS

FEATURE ARTICLE

Plasma based CO_2 and CH_4 conversion: A modeling perspective

Annemie Bogaerts[1]* | Christophe De Bie[1] | Ramses Snoeckx[1] | Tomas Kozák[1,2]

[1] Research Group PLASMANT, Department of Chemistry, University of Antwerp, Wilrijk-Antwerp, Belgium

[2] Department of Physics and NTIS-European Centre of Excellence, University of West Bohemia, Plzen, Czech Republic

***Correspondence**
Annemie Bogaerts, Research Group PLASMANT, Department of Chemistry, University of Antwerp, Universiteitsplein 1, Wilrijk-Antwerp B-2610, Belgium.
Email: annemie.bogaerts@uantwerpen.be

Funding information
Inter-university Attraction Pole (IAP/7), Belgian Federal Office for Science Policy (BELSPO), Francqui Research Foundation, Fund for Scientific Research Flanders, Grant number G.0383.16N; Hercules Foundation, Flemish Government, UAntwerpen

This paper gives an overview of our plasma chemistry modeling for CO_2 and CH_4 conversion in a dielectric barrier discharge (DBD) and microwave (MW) plasma. We focus on pure CO_2 splitting and pure CH_4 reforming, as well as mixtures of CO_2/CH_4, CH_4/O_2, and CO_2/H_2O. We show calculation results for the conversion, energy efficiency, and product formation, in comparison with experiments where possible. We also present the underlying chemical reaction pathways, to explain the observed trends. For pure CO_2, a comparison is made between a DBD and MW plasma, illustrating that the higher energy efficiency of the latter is attributed to the more important role of the vibrational levels.

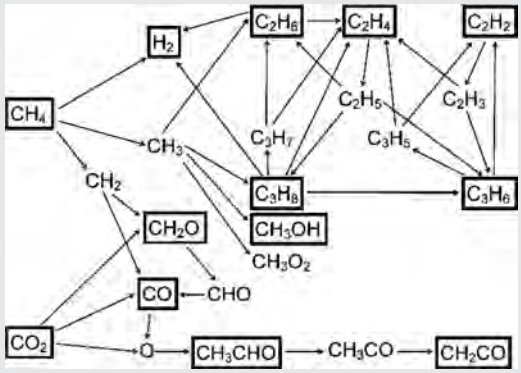

KEYWORDS
0D chemical kinetics model, CO_2 and CH_4 conversion, dielectric barrier discharges, microwave plasmas, plasma chemistry modeling

1 | INTRODUCTION

In recent years, there is increasing interest in plasma used for CO_2 and CH_4 conversion. Several types of plasma reactors are being investigated for this purpose, including (packed bed) dielectric barrier discharges (DBDs),[1–14] microwave (MW) plasmas,[15–20] ns-pulsed,[21] spark,[22–24] and gliding arc (GA)[25–32] discharges. Research focuses on pure CO_2 splitting into CO and O_2, on CH_4 (and other hydrocarbons) reforming, and on mixtures of CO_2 with a hydrogen-source, that is, mainly CH_4, but sometimes also H_2O or H_2, to produce value-added chemicals like syngas, hydrocarbons, and oxygenated products. Key performance indicators are the conversion and the energy efficiency of the process, as well as the possibility to produce specific value-added chemicals with good yields and selectivity. To realize the latter, the plasma should be combined with a catalyst (e.g.,[3–9,33,34]), as the plasma itself is a too reactive environment, and thus produces a wealth of reactive species, which easily recombine to form new molecules, without any selectivity.

To improve the conversion, product yields and energy efficiency of this process, a good insight in the underlying plasma chemistry is crucial. This can be obtained by experiments, but measuring the reactive species densities inside the plasma is far from evident. Therefore, modeling of the plasma chemistry can be a valuable alternative, as it provides information on the most important chemical reaction pathways, and how to tune them to improve the conversion, energy efficiency, and product formation.

In the 80s and 90s, some papers have been published on CO_2 plasma chemistry modeling, with applications to CO_2 lasers.[35–37] These models, however, did not consider the vibrational kinetics, which are important for energy efficient CO_2 conversion.[38] Some other papers have described the vibrational kinetics for gas flow applications,[39,40] but without focusing on the plasma chemistry. In 1981 Rusanov

and Fridman developed a model for CO_2 in a MW plasma, by means of particle and energy conservation equations for the neutral species and an analytical description of the vibrational distribution functions,[41] and they obtained good agreement with experimental values for CO_2 conversion and energy efficiency. However, they did not include the full plasma chemistry with charged species and a self-consistent calculation of the electron density.

In recent years, several plasma chemistry models were presented in literature, for CO_2 splitting,[12,42–46] CH_4 reforming,[47–49] CO_2/CH_4,[50–62] CH_4/O_2,[62–68] CO_2/H_2O,[69] CO_2/H_2,[3] as well as CO_2/N_2[70,71] or CH_4/N_2[72–77] mixtures, because N_2 is one of the most important components in gas effluents. Note, however, that not all these studies were devoted to gas conversion applications. For instance, the CH_4/N_2 mixture is also of interest for cleaning of polluted air streams, plasma assisted ignition and combustion, nitrocarburizing, and for studying the atmospheric chemistry of Titan.[72–77]

As our group PLASMANT has been quite active in this domain in the past few years, this paper gives an overview of recent work carried out in our group, illustrating typical results that have been obtained in terms of gas conversion and energy efficiency, product formation and the underlying chemistry explaining these results, and it will also indicate future challenges for modeling.

We have performed simulations for a DBD and MW plasma, and we will show a comparison between both for pure CO_2 splitting, as they yield very different energy efficiencies, and the latter can be explained from the vibrational kinetics, which are much more important in the MW plasma than in the DBD, as elucidated by the models. To describe these plasma types, two-dimensional or even three-dimensional models would be most accurate; however, as we are interested in the detailed plasma chemistry to reveal the reaction pathways leading to conversion, this would yield excessively long calculation times. Therefore, we typically use 0D modeling, although 1D fluid modeling has also been applied. In the next section, we will briefly describe both the 1D fluid model and the 0D chemical kinetics model, and how the latter can be used to account for spatial effects in a DBD or MW plasma. Furthermore, we will also briefly present the chemistry included in the models. Subsequently, we will show typical results of the models, focusing on pure CO_2 splitting and pure CH_4 reforming, followed by mixtures of CO_2/CH_4, CH_4/O_2 and CO_2/H_2O. We also studied mixtures of CO_2 and CH_4 with N_2,[70,71,77] but this is outside the scope of the present paper. Finally, we will give conclusions and perspectives for future work.

2 | DESCRIPTION OF THE MODELS

A fluid model consists of solving continuity equations for the various plasma species (see next section), with different production and loss terms as defined by the chemical reactions, as well as transport equations based on diffusion and migration in the electric field (the latter only for the charged species). Furthermore, also an energy balance equation is solved for the electrons, to account for the energy gain from the electric field and the energy losses due to collisions. For the other plasma species, the so-called heavy particles, no energy balance equation is needed, as they can be considered in thermal equilibrium with the background gas. Finally, these equations are coupled to Poisson's equation, for a self-consistent calculation of the electric field distribution from the charged species densities. The 1D fluid model used in our work is incorporated in the Plasimo software.[78,79]

In most of our studies, however, we use a 0D model, which is computationally less intensive than a 1D model. Moreover, and more importantly, it allows to account for some spatial effects, characteristic for the type of plasma under study, which are more difficult to (self-consistently) account for in a fluid model, like the occurrence of filaments in a DBD, which is in principle a random process. A 0D chemical kinetics model consists of solving balance equations for the species densities, based on production and loss rates, as determined by the chemical reactions:

$$\frac{dn_i}{dt} = \sum_j \left\{ \left(a_{ij}^{(2)} - a_{ij}^{(1)} \right) k_j \prod_l n_l^{a_{lj}^{(1)}} \right\} \qquad (1)$$

where $a_{ij}^{(1)}$ and $a_{ij}^{(2)}$ are the stoichiometric coefficients of species i, at the left and right hand side of a reaction j, respectively, n_l is the species density at the left-hand side of the reaction, and k_j is the rate coefficient of reaction j (see below).

For each species included in the model, that is, different types of molecules, radicals, ions, excited species, as well as the electrons, a separate balance equation is solved. In the next section, the species included in the models for the different gas mixtures will be outlined.

These balance equations yield the time-evolution of the species densities, averaged over the plasma reactor volume. Indeed, because it is a 0D model, it only accounts for time-variations, while spatial variations, due to transport in the plasma, are not considered. However, based on the gas flow rate, we can translate the time-variation into a spatial variation, that is, as a function of distance travelled through the plasma reactor. This is possible due to the similarity between a batch reactor and a plug flow reactor. Indeed, when the plasma reactor is considered as a plug flow reactor, the temporal variation corresponds to a variation as a function of residence time in the reactor, or in other words, as a function of distance in the reactor.

In this way, we can thus account for spatial variations of input power or gas temperature inside the plasma reactor. Indeed, in a MW plasma, the power deposition is the highest at the position of the waveguide, and as a result, the gas temperature will start to increase around this position. Likewise, as mentioned above, the filamentary behavior of a DBD can be accounted for by applying a number of pulses

as a function of time, which represent the microdischarge filaments inside the DBD reactor. More details about how we account for this filamentary behavior in a DBD can be found in.[42,59,80]

Besides the species densities, also the average electron energy is calculated in this 0D model, based on an energy balance equation, again with energy source and loss terms as defined by the power deposition (or electric field) and the chemical reactions. The average electron energy is used to calculate the energy-dependent rate coefficients of the electron-induced processes, such as ionization, excitation and dissociation. The rate coefficients of the other chemical reactions, that is, between the neutral species or ions, depend on the gas temperature and are calculated from Arrhenius equations, using data adopted from literature.

3 | DESCRIPTION OF THE PLASMA CHEMISTRY INCLUDED FOR THE DIFFERENT GAS MIXTURES

Depending on the gas mixture under consideration, different species need to be considered in the model. Table 1 gives an overview of the species included in the pure CO_2 model, the pure CH_4 model, as well as the extra species included in the CO_2/CH_4, CO_2/H_2O, or CH_4/O_2 gas mixtures. Note that the same species are included in the CO_2/CH_4, CO_2/H_2O, and CH_4/O_2 models, because these combinations indeed yield the production of similar molecules.

As mentioned in the Introduction, the vibrational levels of CO_2 can play an important role in the CO_2 conversion, depending on the type of plasma to be studied. Indeed, while they are of minor importance in a DBD,[42] they are crucial for the CO_2 splitting in a MW plasma.[43,44] This will be further illustrated in section 4.1 below. For this reason, we have developed an extensive chemical kinetics model for CO_2, taking into account these vibrational levels.[43,44] Hence, the symbols "V" and "E" between brackets for CO_2, CO, and O_2 represent the vibrationally and electronically excited levels of these species. For CO_2, most attention is paid to the vibrational levels of the asymmetric stretch mode, which are indeed the most important, as they present the dominant pathway for energy efficient CO_2 splitting (see below). Hence, they are all taken into account, up to the dissociation limit, denoted as CO_2(V1–V21) in Table 1. Furthermore, four

TABLE 1 Overview of the species included in the pure CO_2 model, the pure CH_4 model, as well as the extra species included in the CO_2/CH_4, CO_2/H_2O, and CH_4/O_2 gas mixtures

Molecules	Charged species	Radicals	Excited species
Species in the pure CO_2 model			
CO_2, CO	CO_2^+, CO_4^+, CO^+,	C_2O, C, C_2	CO_2 (Va, Vb, Vc, Vd),
	$C_2O_2^+$, $C_2O_3^+$, $C_2O_4^+$,		CO_2 (V1–V21), CO_2 (E1,
	C_2^+, C^+, CO_3^-, CO_4^-		E2),
			CO (V1–V10), CO (E1–E4)
O_2, O_3	O^+, O_2^+, O_4^+, O^-, O_2^-,	O	O_2 (V1–V4), O_2 (E1–E2)
	O_3^-, O_4^-		
	electrons		
Species in the pure CH_4 model			
CH_4	CH_5^+, CH_4^+, CH_3^+,	CH_3, CH_2, CH, C	CH_4*
	CH_2^+, CH^+, C^+		
C_2H_6, C_2H_4,	$C_2H_6^+$, $C_2H_5^+$, $C_2H_4^+$,	C_2H_5, C_2H_3, C_2H	C_2H_6*, C_2H_4*, C_2H_2*
C_2H_2, C_2	$C_2H_3^+$, $C_2H_2^+$, C_2H^+, C_2^+		
C_3H_8, C_3H_6,		C_3H_7, C_3H_5	C_3H_8*
C_4H_2			
H_2	H_3^+, H_2^+, H^+, H^-	H	H_2*
Extra species in the CO_2/CH_4, CO_2/H_2O, or CH_4/O_2 models			
H_2O, H_2O_2	H_3O^+, H_2O^+, OH^+, OH^-	OH, HO_2	H_2O*
CH_2O,		CHO, CH_2OH,	
CH_3OH,		CH_3O,	
CH_3OOH		CH_3O_2	
C_2H_5OH,		CHCO, CH_3CO,	
C_2H_5OOH,		CH_2CHO, C_2H_5O,	
CH_3CHO,		$C_2H_5O_2$	
CH_2CO			

effective vibrational levels of CO_2, being a combination of the symmetric mode levels, are taken into account, listed in Table 1 as CO_2(Va–Vd), as well as two electronically excited levels of CO_2, denoted as CO_2(E1, E2), ten vibrational levels and four electronically excited levels of CO, presented as CO(V1–V10) and CO(E1–E4), and four vibrational levels and two electronically excited levels of O_2, indicated as O_2(V1–V4) and O_2(E1–E2). More details about these notations can be found in.[43]

For the CO_2/CH_4, CO_2/H_2O, and CH_4/O_2 gas mixtures, no vibrational levels of CH_4 or H_2O are included yet; only some electronically excited levels are considered, denoted with "*." It should, however, be mentioned that these excited levels were only included to describe the energy loss processes, but they were not treated as separate species. Likewise, the CO_2, CO, and O_2 vibrational levels were also disregarded in these mixtures, to reduce the complexity and the calculation time, and because these models were up to now only applied to a DBD plasma. However, we plan to extend these models also to the vibrational levels of CH_4 and H_2O in the future. On the other hand, a large number of higher order hydrocarbons, as well as oxygenates, were included in the models for the CO_2/CH_4, CO_2/H_2O, and CH_4/O_2 gas mixtures, as they are regarded as value-added chemicals. The exact list of plasma species included in each of the models can be consulted in.[12,42–44,49,58–60,62,69]

The species listed in Table 1 might all chemically react with each other. Hence, a large number of chemical reactions (typically up to 1000) are incorporated in these models, including electron impact reactions, electron-ion recombination, ion-ion, ion-neutral, and neutral-neutral reactions. All details about these chemical reaction sets, as well as the corresponding rate coefficients, can be found in.[12,42–44,49,58–60,62,69]

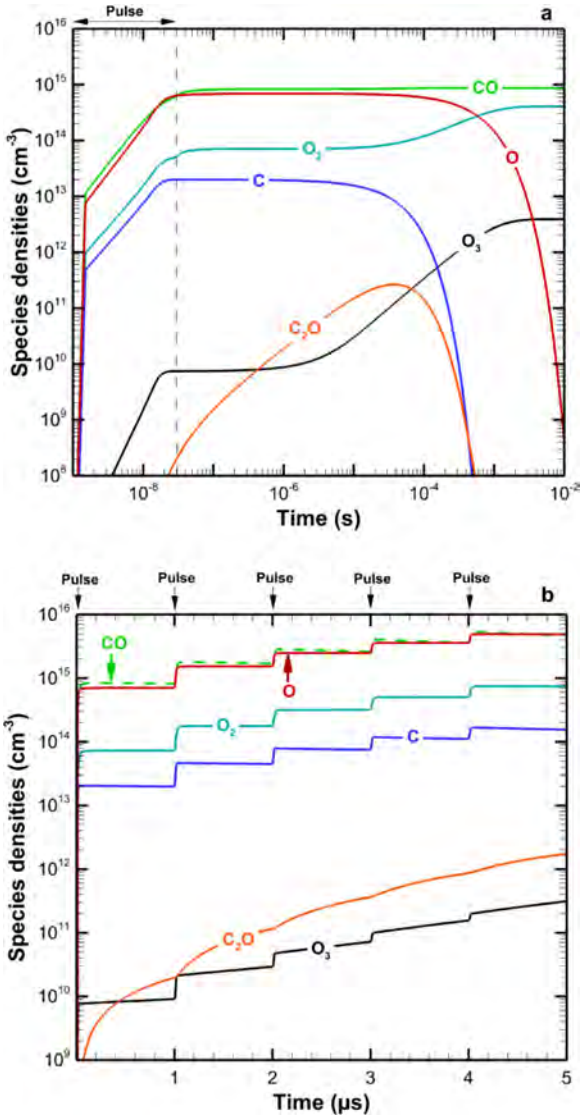

FIGURE 1 Calculated densities of the most important neutral species originating from CO_2 splitting, for one pulse and its afterglow (a), as well as for five consecutive pulses of 30 ns, with an interpulse period of 1 μs (b). The power deposited in the pulses is defined such that it yields typical values for electron density and temperature characteristic for microdischarge filaments (see text). Reproduced with permission,[42] 2012, American Chemical Society

4 | RESULTS AND DISCUSSION

4.1 | Pure CO_2 splitting

4.1.1 | DBD plasma

As explained in section 2 above, the filamentary character of a DBD is accounted for in the 0D model by simulating a large number of microdischarge pulses as a function of time. Details about this approach can be found in our earlier papers.[42,59,80] To illustrate the effect of these successive microdischarge pulses (or filaments) on the chemistry of CO_2 splitting, we plot in Figure 1 the densities of the most important neutral species originating from CO_2, for one pulse and its afterglow (a), as well as for five successive pulses with an interpulse period of 1 μs (b). To mimic typical filament conditions, the power deposition in the pulses was set to a maximum value of 8×10^7 W at 15 ns. This results in a maximum electron density and electron temperature of 1.65×10^{15} cm^{-3} and 2.6 eV, respectively, which are typical values reported in literature for microdischarge filaments.[38] It is clear that the densities of all the products increase during the pulses, and they stay more or less constant in the interpulse period, leading to accumulation of these species (see Figure 1(b)), or they drop if the interpulse period is very long (Figure 1(a)).

The treatment of individual pulses and afterglows also allows us to investigate in detail the underlying chemistry of CO_2 splitting during and in between the microdischarge filaments. Our model reveals that most of the CO_2 splitting occurs during the pulses, in spite of their short duration, and the most important processes at these conditions are electron impact dissociation (with relative contribution of ~52%),

ionization (~29%), dissociative ionization (16%), and dissociative attachment (~23%). Note that the sum of these is larger than 100%. The reason is that the contributions by (dissociative) ionization are partially compensated by the "negative" contribution of ion reactions. Indeed, the ions formed indirectly from CO_2, that is, by electron impact (dissociative) ionization of CO_2, followed by subsequent (charge transfer) reactions, such as $C_2O_4^+$, $C_2O_3^+$, and CO_3^-, will mostly recombine again into CO_2, as illustrated in detail in.[42] Hence, the net contribution to the CO_2 splitting of both ionization processes together is around 23%. Furthermore, our calculations predict that for typical DBD conditions, ~94% of the CO_2 splitting is achieved from the ground state, while ~6% occurs from the vibrationally excited levels (at least for the interpulse period investigated). The reason for this is that the electron temperature in the DBD is too high for efficient vibrational excitation of CO_2.[38,81] More details about these results can be found in.[42]

This 0D model is also extended to simulate the CO_2 conversion during a large number of microdischarge filaments, that is, long time-scale simulations matching the real residence time of the gas in the plasma reactor. The CO_2 conversion and energy efficiency calculated in this way were in very good agreement with the measured data within the SEI range of most practical interest.[12] Therefore, we can use the model to elucidate the most important chemical reactions for CO_2 splitting. The results obtained are the same as for the short time-scale simulations (i.e., one microdischarge filament and its afterglow; see above). Indeed, the most important reactions are electron impact dissociation into CO and O, electron impact ionization into CO_2^+, which recombines with electrons or O_2^- ions into CO and O and/or O_2, and electron dissociative attachment into CO and O^-. These reactions are indicated with thick black arrow lines in the reaction scheme of Figure 2. Although the created CO molecules are relatively stable, at long enough residence time, they can recombine with O^- ions or O atoms, to form again CO_2 (see thin black arrow lines in Figure 2). This is one of the reasons why the CO_2 conversion typically tends to saturate at long enough residence times (corresponding to low gas flow rates).

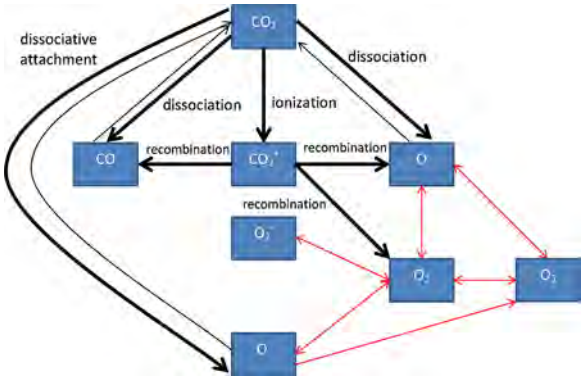

FIGURE 2 Simplified chemical reaction scheme of CO_2 splitting and the further reactions between O, O_2 and O_3 in a DBD plasma, as predicted by our model. The thick black arrow lines represent the most important reactions for CO_2 splitting (mostly attributed to electron impact). The thin black arrow lines point towards the opposite reactions, that is, recombination of CO with either O^- or O, into CO_2. The red arrow lines indicate the conversions between O, O_2 and O_3

However, at short residence times, the O atoms will almost immediately recombine into O_2 or O_3. Moreover, several other reactions can occur between O, O_2 and O_3, possibly also involving the O^- and O_2^- ions, as indicated by the red arrow lines in Figure 2. These reactions will affect the balance between the formation of O_2 and O_3 as stable products, as explained in detail in.[12] Indeed, the selectivity of CO_2 splitting towards CO is always close to 50%, as predicted by our model, but the selectivity towards O_2 formation varies between 45 and 50%, depending on the O_3 production.

4.1.2 | MW plasma and comparison with DBD

Besides calculations for the DBD plasma, we also developed a model for a MW plasma, with special focus on the CO_2 vibrational levels, as explained above. Indeed, the CO_2 vibrational levels are stated to play a very important role for energy efficient CO_2 splitting in a MW plasma.[38] This is indeed also observed in our model results.

In Figure 3, the calculated CO_2 conversion and energy efficiency as a function of SEI are compared for a MW plasma and a DBD reactor, as predicted by our model taking into account the CO_2 vibrational levels. The conversion is calculated by comparing the CO_2 density at the start and the end of the calculations, which correspond in practice to the inlet and the outlet of the reactor. The energy efficiency is obtained here by:

$$\eta(\%) = \frac{\Delta H_R\left(\frac{kJ}{mol}\right) * X_{CO_2}(\%)}{SEI\left(\frac{kJ}{l}\right) * 22.4\left(\frac{l}{mol}\right)} = \frac{\Delta H_R\left(\frac{eV}{molec}\right) * X_{CO_2}(\%)}{SEI\left(\frac{eV}{molec}\right)} \tag{2}$$

where ΔH_R is the reaction enthalpy of the reaction under study (i.e., 280 kJ/mol or 2.9 eV/molec for CO_2 splitting), X_{CO_2} is the CO_2 conversion, and SEI is the specific energy input. The latter can be expressed in kJ/l, like in the left formula, but is also often expressed in J/cm^3 (1 kJ/l = 1 J/cm^3), or in eV/molec, like in the right formula and in Figure 3. The following conversion between both units holds (at atmospheric pressure and room temperature):

$$SEI\left(\frac{eV}{molec}\right) = \frac{SEI\left(\frac{J}{cm^3}\right)}{2.446 \cdot 10^{19}\left(\frac{molecule}{cm^3}\right) \cdot 1.602 \cdot 10^{-19}\left(\frac{J}{eV}\right)} = SEI\left(\frac{J}{cm^3}\right) * 0.255. \tag{3}$$

The SEI is obtained from the deposited plasma power and gas flow rate, as follows:

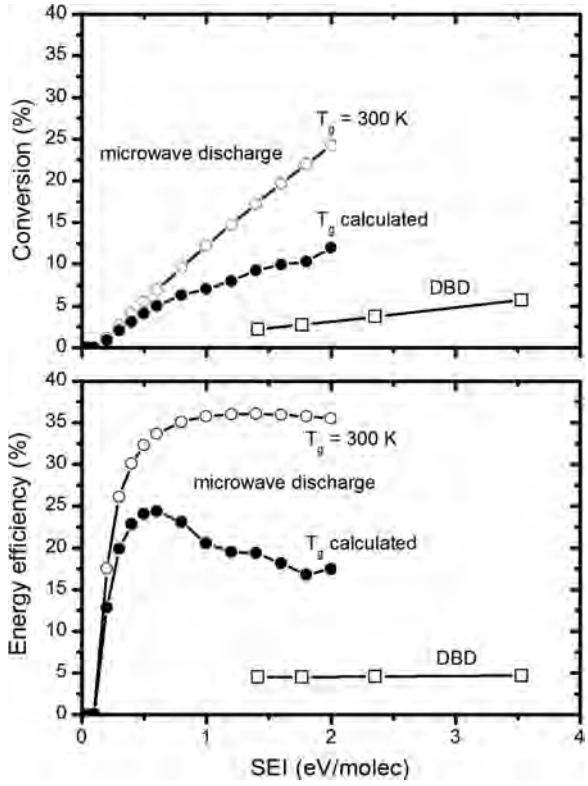

FIGURE 3 Calculated CO_2 conversion (top) and energy efficiency (bottom), in a MW plasma (at 2660 Pa; both for a self-consistently calculated gas temperature as a function of time, reaching values up to 1000 K, and a fixed gas temperature of 300 K) and a DBD plasma (at atmospheric pressure and 300 K), as a function of SEI. Reproduced with permission,[81] 2015, the Royal Society of Chemistry

$$SEI\left(\frac{kJ}{l}\right) = \frac{Plasma\ power\ (kW)}{Flow\ rate\ \left(\frac{l}{min}\right)} * 60\left(\frac{s}{min}\right) \qquad (4)$$

The CO_2 conversion and energy efficiency for the MW plasma, illustrated in Figure 3, are obtained for a self-consistently calculated gas temperature as a function of time (or distance in the reactor), reaching values up to 1000 K,[44] as well as for a fixed gas temperature of 300 K, to allow a more direct comparison with the DBD results, which are also obtained at 300 K. Indeed, the rate coefficients of most chemical reactions are a function of gas temperature, so by comparing at the same temperature, the same reaction rate coefficients are used. Moreover, the gas pressure in the MW plasma was assumed to be 2660 Pa (or 20 Torr), as used in the experiments of,[17] while the DBD results are for atmospheric pressure.

Both the CO_2 conversion and energy efficiency are obviously much higher in the MW plasma than in the DBD, as is clear from Figure 3. Indeed, the maximum conversion in the DBD is only about 5%, at an SEI of 3.5 eV/molec, while the MW plasma with calculated gas temperature up to 1000 K yields a CO_2 conversion of 12% at an SEI of 2 eV/molec, and the conversion at fixed gas temperature of 300 K is even 25%. The higher CO_2 conversion at lower temperature in the MW plasma is attributed to the lower importance of vibrational-translational (VT) relaxation collisions of the CO_2 vibrational levels at lower temperature, which is the most important loss process for the vibrational levels.[43,44]

Also the energy efficiency is much higher in the MW plasma, with values around 35% (when assuming a constant gas temperature of 300 K) and around 25% (for the self-consistently calculated gas temperature), while in the DBD only values around 5% are obtained (more or less independent from the SEI, as the conversion rises proportionally with SEI). In the MW plasma with self-consistently calculated gas temperature, the energy efficiency reaches its maximum at an SEI around 0.6 eV/molec. This is in good agreement with the theoretical and experimental results presented in,[38] although much higher energy efficiencies, up to 80–90%, were reported in.[38]The major effects that limit the maximum energy efficiency in our case, as elucidated by our model, will be discussed below.

The reason for the higher CO_2 conversion and energy efficiency in the MW plasma than in the DBD is the higher population of the CO_2 vibrational levels, as illustrated in Figure 4 for the CO_2 asymmetric mode levels (i.e., the mode which is most important for CO_2 splitting[38,43,44]). In the MW plasma the vibrational population drops gradually upon the higher vibrational levels, yielding a vibrational temperature of 4115 K, while in the DBD, the vibrational population drops over several orders of magnitude compared to the ground state density, even for the lowest levels, and the vibrational temperature is calculated to be only 961 K. Thus, in the DBD the CO_2 splitting is mainly attributed to electron impact excitation-dissociation from the CO_2 ground state (see also previous section), while in the MW plasma, the CO_2 splitting is induced by electron impact vibrational excitation of the lowest vibrational levels, followed by vibrational-vibrational (VV) collisions, gradually populating the higher

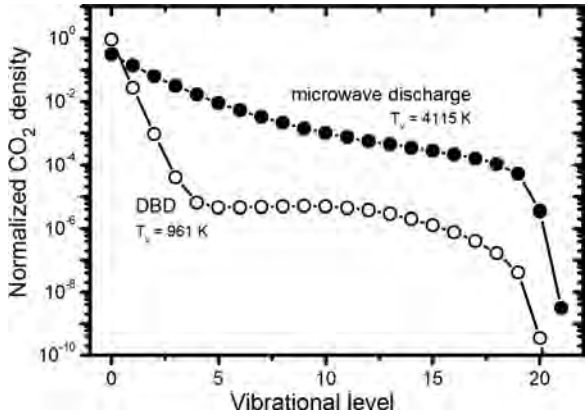

FIGURE 4 Normalized vibrational distribution function of the asymmetric mode levels of CO_2 in a MW plasma (at 2660 Pa and self-consistently calculated gas temperature) and a DBD (at atmospheric pressure and 300 K), at an SEI of 0.6 eV/molec, both taken at the time of maximum vibrational temperature. Reproduced with permission,[81] 2015, the Royal Society of Chemistry

vibrational levels, leading to dissociation of CO_2. This stepwise vibrational excitation, or so-called "ladder-climbing" process, explains the higher CO_2 conversion and energy efficiency in the MW plasma. Indeed, this process only requires 5.5 eV for dissociation, while electron impact excitation-dissociation requires 7–10 eV, as it proceeds through a dissociative electronically excited level of CO_2.[38,81] This "waste of energy" explains the lower energy efficiency in a DBD plasma.

The best energy efficiency predicted by our model for a MW plasma, for the conditions under study, was around 32%.[44] In literature, much higher values were reported, that is, back in 1983, values up to 80% were obtained by Fridman and colleagues for subsonic flow, and up to 90% for supersonic flow conditions.[15,38] More recently, researchers from DIFFER obtained values up to 55%[18] and 45%[20] at reduced pressure, and up to 50% for reverse vortex flow and atmospheric pressure.[19] As these values are clearly higher than the best values obtained by our model, we have analyzed how the vibrational energy of CO_2 is consumed by individual reactions, to better understand the limitations in the energy efficiency. Our calculations reveal that maximum 60% of the energy available in the CO_2 vibrational levels can be used for CO_2 dissociation, while the rest is mainly lost by VT relaxation, giving rise to gas heating. Because a higher gas temperature gives rise to higher VT relaxation rates, we should keep the gas temperature as low as possible, to minimize VT relaxation losses in the vibrational population. This was also obvious from Figure 3 above. For the same reason, the energy efficiency typically drops upon increasing gas pressure, because of the increasing V-T relaxation processes. By using a fast gas flow or pulsed power operation, we expect that these losses can be reduced, thereby possibly further increasing the energy efficiency.

In principle, one could argue that a higher gas temperature might yield a higher equilibrium vibrational population, based on statistical thermodynamics grounds, and moreover, the rate coefficients of the CO_2 dissociation reactions increase with gas temperature. Thus, one might expect that a higher gas temperature could result in a better energy efficiency. If this would be true, it would be beneficial to heat the CO_2 gas before entering the plasma reactor, to make use of the vibrational population in a plasma. Therefore, we have performed calculations to investigate the effect of the initial CO_2 gas temperature on the CO_2 conversion and energy efficiency in a MW plasma, in a wide range from room temperature to 2000 K; see Figure 5(a). The initial CO_2 vibrational population was set according to a Boltzmann distribution at the given temperature. The calculations were performed for a fixed SEI (in the plasma) of 1 eV/molec, but the energy needed to preheat the gas was added to this SEI, and the sum of both was used to evaluate the energy efficiency (see the formula above).

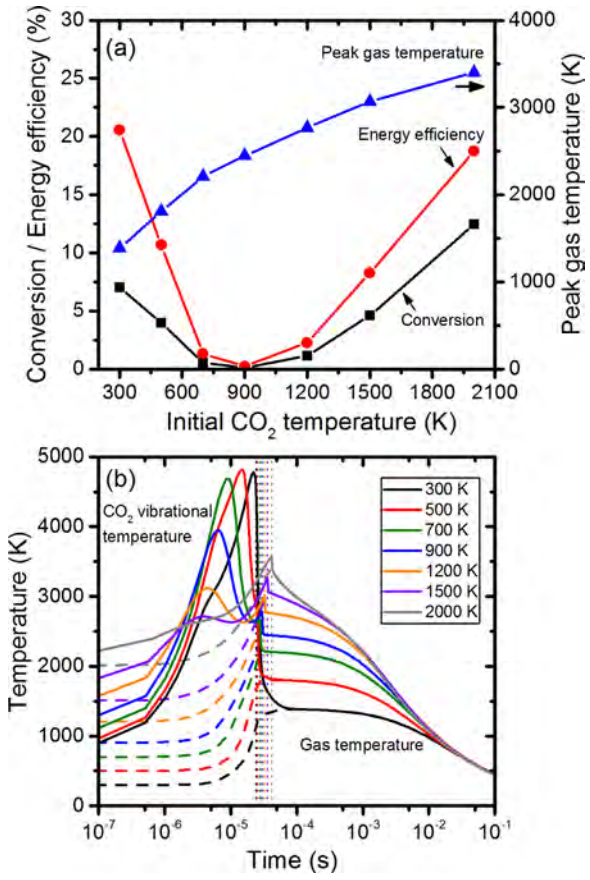

FIGURE 5 (a) Calculated CO_2 conversion and energy efficiency (left axis) as a function of initial CO_2 gas temperature entering the plasma, in a MW plasma at SEI of 1 eV/molec, $p = 100$ Torr and E/N = 50 Td. The corresponding calculated peak gas temperature in the plasma is also plotted (right axis). (b) Time-evolution of the vibrational temperature and gas temperature in the plasma, for each initial gas temperature. The small dashed vertical lines in Figure 5(b) indicate the residence time of the gas in the active plasma phase, or in other words, the end of the microwave power pulse and the beginning of the afterglow. Note that this residence time is slightly different for the different conditions of initial gas temperature, because the latter affects the gas density, while the gas flow rate is fixed

When starting with room temperature CO_2, the conversion and energy efficiency are calculated to be 7% and 20%, respectively, as was also observed in Figure 3 above. However, when rising the initial CO_2 temperature to 900 K, the conversion and energy efficiency virtually drop to zero. Thus, the effect of the higher equilibrium vibrational population due to a higher initial gas temperature is clearly compensated by the increased VT relaxation rates in this temperature range. This stresses again the importance of keeping the gas temperature as low as possible for energy efficient CO_2 conversion. For temperatures above 1000 K, the conversion and energy efficiency again start to increase with temperature, because the equilibrium vibrational population gradually becomes more and more important. However, only at an initial gas temperature of 2000 K, the obtained CO_2 conversion and energy efficiency become comparable to the values reached at an initial gas temperature of 300 K.

The maximum gas temperature in the plasma, as calculated for the various cases of initial gas temperature, is also depicted in Figure 5(a). Moreover, in Figure 5(b), the time-evolution of the vibrational temperature and gas temperature in the plasma is plotted, for each initial gas temperature. It is clear that during the active plasma phase, that is, when the microwave power is applied, the vibrational temperature is much higher than the gas temperature, indicating that the vibrational distribution function (VDF) is far from thermal equilibrium. When the microwave power is switched off, that is, in the so-called afterglow, indicated in Figure 5(b) by the small dashed vertical lines for each initial gas temperature, the vibrational temperature drops and becomes equal to the gas temperature. The characteristic relaxation time due to VT relaxation, which is the most important for thermalization of the VDF, can be estimated from the inverse of the product of the CO_2 gas density with the relaxation rate constant for VT relaxation from the first vibrational level, as in.[43] This yields a value in the order of 10^{-4} s at an initial gas temperature of 300 K, but this value clearly drops with increasing initial gas temperature (because the latter determines the gas density), reaching about 10^{-5} s at 700 K, 10^{-6} s at 1200 K, and 10^{-7} s at 2000 K. This explains why in Figure 5(b) the peak in the vibrational temperature is reached earlier in time at higher initial gas temperature. Of course, in the model, thermalization of the VDF does not only occur by VT relaxation from the first vibrational level, and the higher vibrational levels also contribute to the relaxation, so the situation in Figure 5(b) is more complicated, but at least the above values give an indication on the relaxation times.

Note that only at the highest initial gas temperature of 2000 K, the vibrational and gas temperature in the active plasma phase are more or less comparable. Indeed, the calculated maximum gas temperature now reaches 3400 K, while the maximum vibrational temperature is 3500 K. Hence, at this stage, the VDF, and the plasma in general, almost reach thermal equilibrium. The higher CO_2 conversion and energy efficiency observed in Figure 5(a) is now due to the higher dissociation rates at higher temperature, but it is important to realize that the advantage of a non-equilibrium plasma for selective electron impact excitation to the CO_2 vibrational levels is lost. Note that the CO_2 conversion and energy efficiency obtained in this case are lower than the theoretical thermodynamic equilibrium limits, which are about 60% conversion and 55% energy efficiency at a temperature of 3400 K. The reason is that in our case, the value of 3400 K is only the peak value (see Figure 5(b)), and at lower temperatures, the backward reaction of CO into CO_2 due to recombination becomes important, thus limiting the net conversion and energy efficiency.

Finally, we have looked at the underlying plasma chemistry of CO_2 splitting in a MW plasma, to elucidate how the CO_2 conversion and energy efficiency could be further enhanced. Our model predicts that the energy efficiency is strongly affected by the reaction chemistry of the O atoms formed by CO_2 splitting. Ideally, these O atoms should be entirely used for further dissociation of CO_2 (i.e., $CO_2 + O \rightarrow CO + O_2$) instead of recombining with other O atoms into O_2, in order to obtain the highest energy efficiency. The above dissociation reaction indeed seems to limit the attainable energy efficiency, as its rate constant is characterized by a rather high activation energy (1.43 eV). Note that this activation energy applies to the reaction for ground state CO_2 molecules. In our model, the same reaction is also included for CO_2 molecules in vibrational levels, and in that case, the rate constant for this reaction, as well as for all other reactions in our model by CO_2 vibrational levels, is characterized by a somewhat lower activation energy. Indeed, the activation energy for reactions with CO_2 vibrational levels is reduced to account for the energy of the vibrational levels, by means of the so-called Fridman-Macheret α model,[38] as described in detail in.[43] For the above reaction, a correction factor $\alpha = 0.5$ is used. This indeed yields lower activation energies in the order of 1.29, 1.14, 1.00, 0.86, and 0.72 eV, for the first five vibrational levels with energies of 0.29, 0.58, 0.86, 1.14, and 1.43 eV, respectively.

When artificially lowering the activation energy for this reaction from 1.43 eV (for the CO_2 ground state) to the theoretical minimum of 0.35 eV (dictated by the reaction enthalpy), the rate of this reaction increases by six orders of magnitude, and the highest energy efficiency of CO_2 splitting, as predicted by the model, rises from 30 to 52%, which is close to the highest values reported by researchers from DIFFER[18–20] (cf. above). Hence, this indeed points out that the further dissociation reaction upon collision with O atoms might be the limiting factor in determining the overall energy efficiency, and we should look for conditions that can enhance this reaction, at the expense of the recombination of two O atoms into O_2.

4.1.3 | Product separation

The previous example illustrates how modeling can give insight in the underlying chemical reactions, which can be used to look for possible solutions to improve the performance. A similar example will be given here, for the product separation of CO_2 splitting into CO and O_2. Indeed, this separation might not be straightforward, especially for separating O_2 from CO and unreacted CO_2, as the common separation techniques, such as centrifugation, distillation and absorption, are difficult and energy-intensive, due to the small difference in molar mass between CO and O_2. Furthermore, electrolytic membranes, with a conductivity towards O_2, require high temperatures, again limiting the energy efficiency in combination with low-temperature plasmas.[82]

We have computationally investigated that adding a H-containing gas, such as H_2 or CH_4, to the CO_2 plasma might provide a solution for separating the reaction products.[83] Indeed, in this way the O atoms, produced

from CO_2 splitting, can be chemically trapped, because they recombine faster with H atoms into OH radicals, which subsequently react further into H_2O than that they would recombine with another O atom into O_2. This chemical way of trapping the O_2 could be a simpler and more energy efficient way of separating the reaction products, because H_2O can be easily removed from the gas mixture, and the CO/CO_2 mixture can be separated with existing membrane technology.[84]

As illustrated in Figure 6, adding a small amount of H-containing gas, more specifically 3% of H_2 or 2% of CH_4, is sufficient to completely trap the oxygen into the formation of H_2O, although it needs to be mentioned that this was only investigated for a limited CO_2 conversion of only a few%. However, these simulations show the potential of this idea. Moreover, our model predictions were also experimentally validated for CH_4 addition (see more details in[83]).

A critical note to these observations is that adding H_2 or CH_4 to the plasma sacrifices the overall energy efficiency of the CO_2 conversion, because not all the energy put into the plasma can be used for CO_2 splitting and some energy is now also consumed by the H_2 or CH_4 gas. In ref.[83] we have calculated the energy cost of pure CO_2 splitting, and we have compared it to the corresponding values when 3% H_2 or 2% CH_4 was added. It was shown that the addition of a trapping gas (CH_4 or H_2) leads to a small reduction of the CO_2 conversion, as indeed some fraction of the plasma power is consumed by the trapping gas, and this results in a slightly higher energy cost (i.e., about 10–20%) for CO production. However, we need to compare this slightly higher energy cost for CO production within the plasma with the energy requirements for the gas separation of the exit gas stream. The latter was also estimated in ref.,[83] based on available data in literature, and it was concluded that this energy cost for gas separation is clearly higher than the energy cost for CO production in the plasma, even when adding a trapping gas.[83] Moreover, the membrane technology for separating the $CO/CO_2/O_2$ mixture is still under development. Therefore, we believe, based on these estimates and considerations, that this chemical trapping method might be a promising, energy efficient alternative to gas separation methods."

Finally, this idea also has some potential for enhancing the CO_2 conversion according to Le Chatelier's law, by removing the O_2 from the plasma, which has already been demonstrated in literature for a hybrid DBD reactor with a solid oxide electrolyser cell.[85]

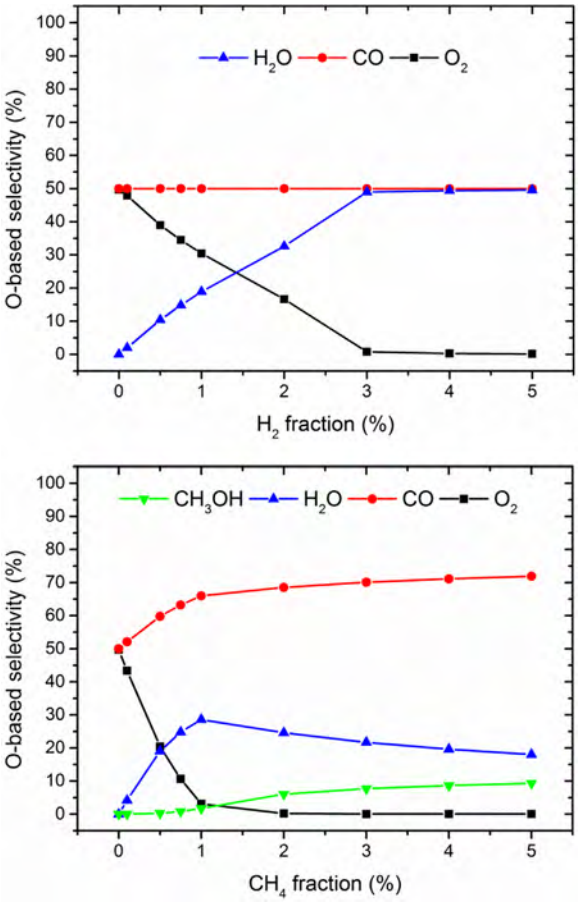

FIGURE 6 Calculated O-based selectivities of the reaction products of CO_2 splitting, upon addition of a few% of H_2 (top) or CH_4 (bottom), illustrating that O_2 is completely removed (or trapped into H_2O), after 3% of H_2 addition or 2% of CH_4 addition. Reproduced with permission,[83] 2014, Wiley

4.2 | CH_4 reforming

The process of CH_4 reforming in a DBD reactor was studied with a 1D fluid model.[49] Figure 7 shows the calculated densities of CH_4 and of the various molecules formed out of the CH_4 conversion, as a function of residence time, for a DBD reactor operating at 6 kV and 10 kHz. The residence time of 20 s corresponds to a gas flow rate of 50 mL/min for the setup under consideration.[49] It is clear that CH_4 is gradually converted into other molecules, such as H_2, C_2H_6, C_2H_4, C_2H_2, C_3H_8, and C_3H_6. The conversion is most

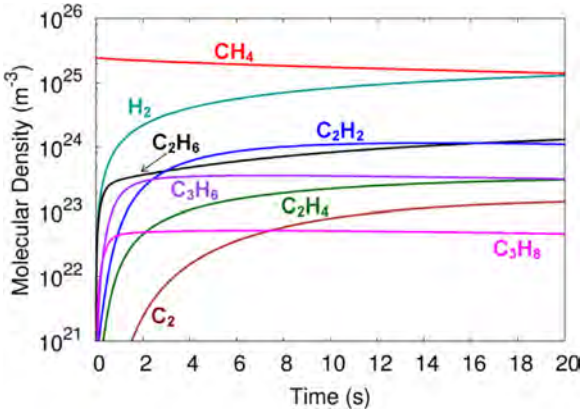

FIGURE 7 Calculated densities of CH_4 and the various molecules formed out of the CH_4 conversion, as a function of residence time, for a DBD reactor operating at 6 kV and 10 kHz. Reproduced with permission,[49] 2011, Wiley

pronounced in the first 1–2 s. From these densities, the CH_4 conversion and the yields of the various products can be calculated. The model predicts that 40% of CH_4 is converted after 20 s, and the H_2 and C_2H_y molecules are formed with the highest yields, being about 20% after 20 s. The yield of the C_3H_y hydrocarbons is about 5% after 20 s. Comparison with experimental data for the same conditions, performed by Verheyde and Paulussen, showed reasonable agreement, as illustrated in detail in ref.[49]

This good correlation with experimental data indicates that the model captures the right chemical processes, and can thus be used to obtain more insight in the dominant reaction pathways for the conversion of CH_4 into higher hydrocarbons and H_2, as is illustrated in Figure 8. The model reveals that the conversion is initiated by electron impact dissociation of CH_4 into CH_3 radicals, which will recombine into higher hydrocarbons, such as C_2H_6 and C_3H_8. These hydrocarbons, as well as CH_4 itself, will also dissociate into H_2 formation. Moreover, various dissociation and recombination reactions lead to the other, unsaturated hydrocarbons. The H atoms are not included in this figure, because they react with most hydrocarbon molecules and radicals, and including them would make the figure too messy, with too many arrows pointing between the various species. The most important reactions for the H atoms are three-body recombination reactions with C_2H_4 and C_2H_2 molecules (rate $\sim 10^{18}$ cm^{-3} s^{-1}), and to a lower extent also with C_2H_5 and C_2H_3 radicals (rate $\sim 10^{16}$ cm^{-3} s^{-1}), towards C_xH_{y+1} species. Recombination of two H atoms into H_2 by a three-body reaction is not important (rate $\sim 10^{12}$ cm^{-3} s^{-1}). Details about the exact reaction mechanisms can be found in ref.[49]

4.3 | CO_2/CH_4 mixture

We also applied the same 1D fluid model to a DBD reactor in a CO_2/CH_4 mixture. Indeed, besides pure CO_2 splitting and CH_4 reforming, the simultaneous conversion of CO_2 and CH_4, that is, so-called dry reforming of methane (DRM), is also of great interest, because it allows to convert two greenhouse gases at the same time, and more importantly, it might allow to produce some value-added chemicals, like syngas (CO/H_2), methanol, formaldehyde, formic acid, etc. The densities of CO_2, CH_4, and the various molecules formed out of this mixture are plotted in Figure 9, as a function of the initial CO_2 fraction in the mixture, for a gas residence time of 5 s (which corresponds to a gas flow rate of 200 mL/min for the reactor setup under study; see details in[49,62]). The top panel of Figure 9 illustrates again that several higher hydrocarbons are formed out of CH_4 with rather high densities. Nevertheless, the major products of the CH_4/CO_2 conversion are CO and H_2, or syngas, as shown in the middle panel. The H_2/CO ratio is found to be higher than one in the entire CO_2/CH_4 mixing ratio. Besides, also H_2O is formed in non-negligible amounts, as well as some oxygenates, such as

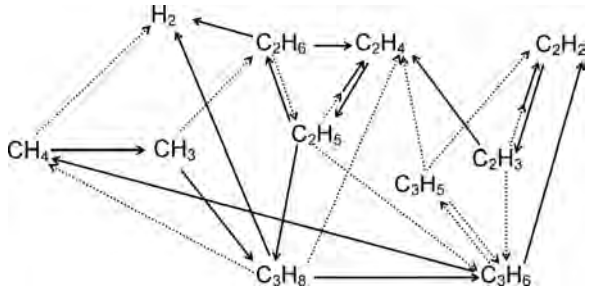

FIGURE 8 Schematic overview of the dominant reaction pathways for the conversion of CH_4 into higher hydrocarbons and H_2. The most important reactions are indicated with a solid line, while the dashed lines represent the less important reactions

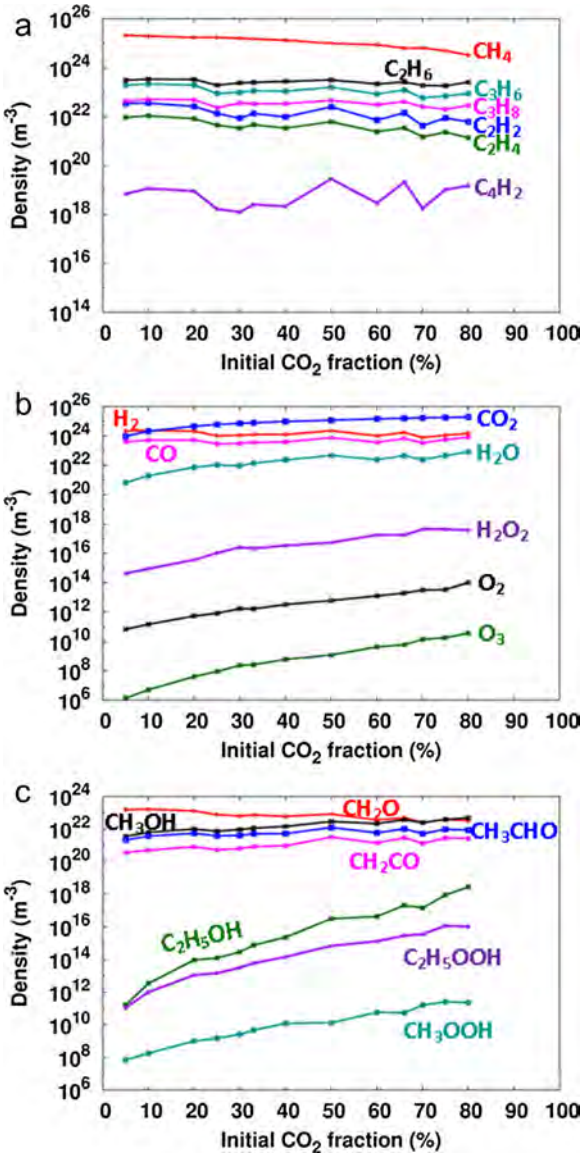

FIGURE 9 Calculated densities of CH_4 and CO_2, as well as the various molecules formed out of the CH_4 and CO_2 conversion, after a residence time of 5 s, as a function of initial CO_2 fraction in the CO_2/CH_4 mixture, for a DBD reactor operating at 5 kV and 10 kHz

methanol (CH_3OH), formaldehyde (CH_2O), acetaldehyde (CH_3CHO), and ketene (CH_2CO) (see bottom panel).

These results could not directly be compared with experimental data at the same conditions, but they are in reasonable agreement with results from literature, for quite similar conditions, as presented in detail in ref.[62]

The conversion of CH_4, after this residence time of 5 s, is calculated to be about 10% for a CO_2 fraction up to 30–40%, but it increases to about 35% for a CO_2 fraction of 80%. This is attributed to the increasing importance of the loss reaction of CH_4 with CO_2^+ ions, as explained in detail in.[62] The CO_2 conversion is calculated to be much lower than the CH_4 conversion, that is, only a few%. This is because the above reaction between CH_4 and CO_2^+ ions results in CO_2 formation, explaining the low net conversion. However, the CO_2 conversion increases to about 20% at a CH_4 fraction of 95%, because of the additional loss processes of CO_2 upon collision with (mainly) CH_2 radicals.

From the calculated densities of the various molecules (as plotted in Figure 9), their yields can also be deduced. The maximum yields of H_2, CO, formaldehyde, and methanol are found to be 34, 10, 0.9, and 0.4%, respectively. These maximum values are, however, not reached at the same gas mixing ratios. Indeed, the maximum yields of H_2 and CO are reached at a 20/80 CH_4/CO_2 mixture, while the optimum CH_4/CO_2 gas mixing ratios for formaldehyde and methanol formation are found to be 90/10 and 25/75, respectively. Also the residence time at which these maximum yields are reached, are not always the same. The maximum yield of formaldehyde is typically reached at lower residence times (order of 10 s), indicating that it easily reacts further or is decomposed into CO, CO_2, and H_2O.[62] The above mentioned yields of formaldehyde and methanol correspond to selectivities of only a few%. Thus it is clear that when the selective production of these oxygenates is targeted, the plasma will have to be combined with a specific catalyst.

The dominant reaction pathways for the conversion of CO_2 and CH_4 into H_2, CO, higher hydrocarbons and oxygenates are illustrated in Figure 10. The thickness of the lines corresponds to the "importance" of the reaction. The dissociation of CH_4 is initiated by electron impact, forming CH_3 radicals, which recombine into higher hydrocarbons, in the same way as explained in previous section for the pure CH_4 plasma. Note the thick arrow line from C_2H_4 to C_2H_5, indicating the high formation rate of this radical. This is partially reflected in its rather high density compared to other radicals (see[62]), but on the other hand, this is virtually the only production mechanism for this radical, while it easily reacts further into C_2H_6 and C_3H_8, as is clear from Figure 10. Thus, it mainly serves as intermediate for the back reaction from C_2H_4 into C_2H_6, after C_2H_6 was first converted into C_2H_4 (see Figure 10).

It is also clear from Figure 10 that electron impact dissociation of CH_4 and of the higher hydrocarbons also

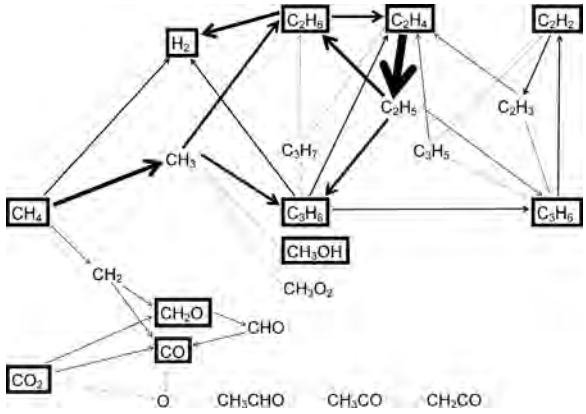

FIGURE 10 Schematic overview of the dominant reaction pathways for the conversion of CH_4 and CO_2 into higher hydrocarbons, H_2, CO, and higher oxygenates, in a 70/30 CH_4/CO_2 DBD plasma, operating at 5 kV and 10 kHz. The thickness of the arrow lines is correlated to the importance of the reaction path

yields the formation of H_2, like in the case of the pure CH_4 plasma (see above). However, in the CO_2/CH_4 plasma, the CH_3 radicals do not only create higher hydrocarbons, but they also form methanol (CH_3OH) and CH_3O_2 radicals, albeit to a lower extent. Moreover, the CH_2 radicals, also created from electron impact dissociation of CH_4, react with CO_2 to form formaldehyde (CH_2O) and CO. Finally, the O atoms, created from electron impact dissociation of CO_2 (see Figure 2 above), also initiate the formation of higher oxygenates, like acetaldehyde (CH_3CHO), which reacts further into CH_3CO radicals, and the latter can be further converted into ketene (CH_2CO). However, these pathways are not so important in absolute terms, as indicated by the thin dashed lines in Figure 10.

Besides the 1D fluid model, we also developed a 0D chemical kinetics model for a CO_2/CH_4 mixture, focusing on the detailed plasma chemistry of one microdischarge pulse and its afterglow, as well as five consecutive microdischarge pulses, to study the detailed plasma chemistry during and in between the filaments. Like explained in the section on pure CO_2 splitting, the power deposition in the pulses is again defined in such a way that it yields typical electron density and temperature values for microdischarge filaments.[38]

A reaction path analysis reveals that electron impact reactions are again dominant during the microdischarge pulses, but chemical reactions with radicals are of primary importance in between the pulses (i.e., the so-called afterglows). During the pulses, the CH_4 dissociation is much more pronounced than the CO_2 dissociation, but in the afterglows, nearly 74% of the dissociated CH_4 is formed again, by recombination of CH_3 radicals with H atoms. The CO_2 dissociation, on the other hand, proceeds further in the afterglows: about 22% of the overall CO_2 dissociation occurs during the pulses, while 78% takes place in the afterglows, due to reactions between CO_2 and CH_2 radicals, as also

mentioned above. More details about these reaction processes can be found in ref.[59]

Furthermore, the model was also applied to perform long time-scale simulations, corresponding to real residence times, to predict the CO_2 and CH_4 conversion and the energy efficiency. These results are plotted as a function of SEI in Figure 11, along with experimental data, obtained from Tu and coworkers (University of Liverpool). A good agreement is reached between calculation results and experiments, indicating that the model captures the most important plasma chemistry.

At a CO_2/CH_4 mixing ratio of 50/50, the CO_2 conversion is at maximum 30% in the SEI range under study, while the CH_4 conversion reaches values up to 50%, at the maximum SEI investigated. The reason for the higher CH_4 than CO_2 conversion is again the charge transfer reaction between CO_2^+ ions and CH_4 mentioned above, yielding CH_4^+ ions and CO_2. Hence, this reaction promotes the CH_4 conversion, and it reduces the effective net CO_2 conversion, because otherwise the CO_2^+ ions might dissociatively recombine with electrons or O_2^- ions into CO and O and/or O_2, thus contributing to the CO_2 conversion, as explained in the section on pure CO2 splitting above.

This example illustrates that computer modeling can be very useful for obtaining a more detailed understanding of the underlying chemical processes, and that it might also be used for optimizing the experiments, e.g., by selecting plasma conditions which suppress the above reaction, when aiming to promote the CO_2 conversion more than the CH_4 conversion.

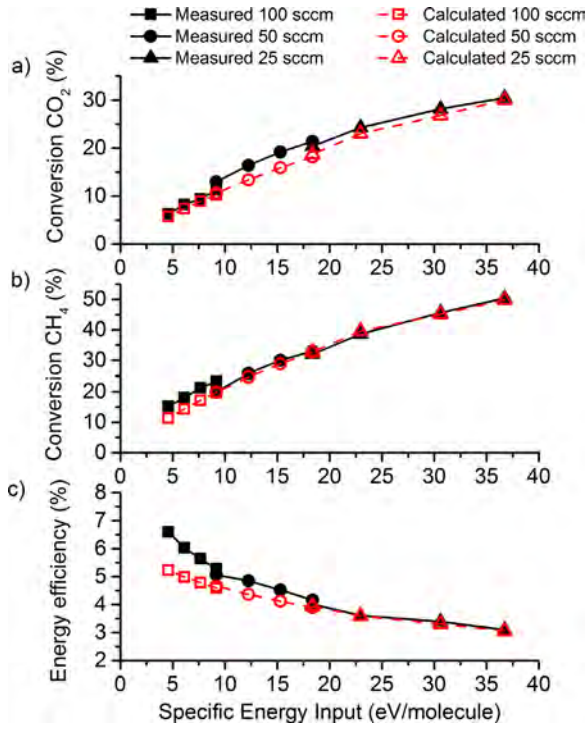

FIGURE 11 Measured (solid, black lines) and calculated (dashed, red lines) CO_2 conversion (a), CH_4 conversion (b) and overall energy efficiency (c) in a DBD plasma used for DRM, as a function of the SEI, at a 50/50 CO_2/CH_4 mixture

Next to the CO_2 and CH_4 conversion, also the selectivities of the reaction products can be calculated. Again, syngas is the major reaction product, as well as (to a lower extent) formaldehyde, methanol, C2 and C3 hydrocarbons. In the case of a 50/50 CO_2/CH_4 mixture, the selectivities towards H_2 and CO formation are calculated to be 55 and 48%, the C2 and C3 hydrocarbons are formed at a selectivity of 6 and 30%, and the selectivities for the formation of formaldehyde and methanol amount to 13 and 3%, respectively. Note that the sum of the selectivities is above 100%, which is due to the definitions used (see details in ref.[59]). In this 50/50 CO_2/CH_4 mixture, the syngas is formed in a H_2/CO ratio of ~ 1.5, which is of considerable interest for the chemical industry. Also the direct formation of methanol and formaldehyde, without the need of an intermediate (syngas) step, is interesting, although the selectivities towards these products are too low to be of practical interest. For this purpose, the combination with a catalyst will be necessary, as already mentioned above.

The energy efficiency obtained in this case is around 6.6% at a low SEI of 4.6 eV/molec, as appears from Figure 11(c), and drops to 3.1% at the highest SEI investigated (36.7 eV/molec). This illustrates the trade-off between conversion and energy, as the conversion reaches its maximum at high SEI, while the opposite behavior is observed for the energy efficiency. The reason for this trade-off can be easily understood from Eq. (2) above, which indicates that the energy efficiency is proportional to the conversion, but inversely proportional to the SEI. The conversion typically rises with the SEI, because there is more energy available for dissociation, but if the conversion rises less rapidly than the values of the SEI, the energy efficiency will drop upon rising SEI, following Eq. (2). This is exactly the case for the data of Figure 11.

When we compare the obtained energy efficiencies with values estimated for the classical DRM process (i.e., based on a thermodynamic calculation for heating the gas and for reaching a conversion of 72% (CH_4) and 82% (CO_2), which gives a theoretical maximum achievable energy efficiency of 58%; see details in ref.[59]), it is clear that the energy efficiency presented in Figure 11(c) is not yet competitive with the classical DRM process. However, it needs to be mentioned that the results presented in Figure 11 served mainly to validate the model, which was developed to better understand the underlying chemistry, but the conditions under study were not yet optimized in terms of highest conversion and energy efficiency.

Thus, in order to find out whether a DBD plasma might eventually be competitive with the classical DRM process, we performed an extensive computational optimization study, to identify the effect of various operating parameters, like the CO_2/CH_4 gas mixing ratio, the power, the residence

time and the frequency (defining the number of micro-discharge filaments in the reactor for a given gas residence time). The aim was to investigate which of these parameters yields the most promising results and whether these results would be good enough for industrial exploitation. The computations were again validated by experiments, although this was only possible in a somewhat limited parameter range.[60] From the good agreement reached between the calculations and experiments, we can be confident about the predictive nature of our model, and thus we can use it in a wider parameter range, beyond what is typically accessible for the most common experiments. This allows us to find out whether such operating conditions can give better results than the current state-of-the-art. The result of this comprehensive study, which was based on a total of 750 simulations,[60] is summarized in Figure 12. This figure shows the maximum and minimum obtained values of total conversion versus energy efficiency, for all conditions investigated.

Our calculations predict that an SEI of 100 J/cm^3, a CO_2/CH_4 ratio of 90/10, a frequency of 10 Hz and a residence time of 1 ms yield the best results in terms of both conversion and energy efficiency. The total conversion (i.e., average value of the CO_2 and CH_4 conversion) is 84% in this case, and it corresponds to an energy efficiency of 8.5%. In general, a higher CO_2 content in the gas mixture yields a higher total conversion and energy efficiency. Furthermore, as illustrated also above, a higher SEI leads to a higher conversion, but at the expense of the energy efficiency. Nevertheless, the drop in energy efficiency is not as dramatic as the rise in conversion, and therefore, higher SEI values give rise to the best overall results.

The maximum energy efficiency predicted by these simulations is between 11.4 and 15.1%, depending on the gas mixing ratio, and is obtained at the lowest SEI values investigated, thus corresponding to a low conversion (see Figure 12). Although these energy efficiencies are better than the values reported up to now for DRM in a DBD plasma (see detailed comparison in ref.[60]), it is still significantly lower than the theoretical maximum achievable energy efficiency of classical DRM (58%; see above), suggesting that a DBD plasma is not yet competitive for industrial implementation. The main reason for this, as mentioned in the section on pure CO_2 splitting above, is that electron impact excitation-dissociation, which is the dominant dissociation process in a DBD, is limiting the energy efficiency. Indeed, it requires an electron energy of about 7–10 eV, while in principle only 5.5 eV is needed for CO_2 dissociation.[38,81] Thus, there is "waste of energy" when going through the excitation-dissociation channel, and this explains the limited energy efficiency of a DBD plasma, in contrast to a MW plasma, where vibrational excitation, followed by VV collisions, gradually populating the higher vibrational levels (i.e., so-called ladder-climbing), finally leading to dissociation, is the main dissociation channel, and exactly needs only this 5.5 eV.[38,81]

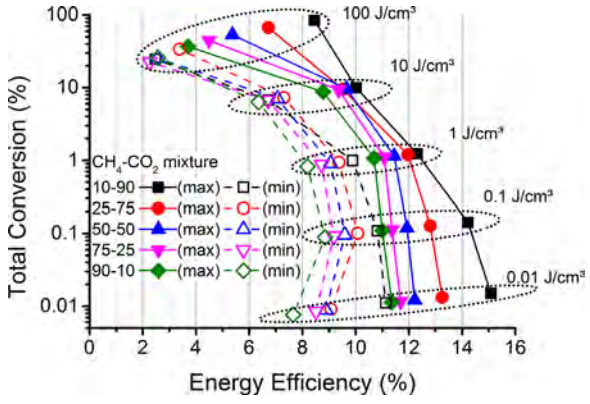

FIGURE 12 Maximum (solid lines) and minimum (dashed lines) achieved values of total conversion versus energy efficiency, as obtained from the calculations for a wide range of operating conditions in a DBD plasma. In total, 750 different conditions were investigated. The different curves represent the different CH_4-CO_2 gas mixing ratios (see legend). The different SEI values, giving rise to these results, are identified with the labels next to the curves

However, the classical DRM process will probably also not reach this theoretical maximum of 58% in practice, because this value for instance does not yet account for the thermal efficiency of the heaters. Furthermore, a DBD has other advantages, such as its flexibility (e.g., when combined with peak currents from renewable energy sources), its ease of use and possibilities for upscaling, as well as for the combination with catalysis, opening perspectives for the selective production of value-added chemicals. Moreover, when a catalyst is inserted as a packing in the DBD reactor, the conversion and energy efficiency rise significantly,[10,14] so that this process hopefully still becomes competitive in the future, although much more research will be needed for this purpose.

4.4 | CH_4/O_2 mixture

To compare the production of value-added chemicals in a CO_2/CH_4 mixture and a CH_4/O_2 mixture, we also applied our 1D fluid model to a DBD reactor in a CH_4/O_2 mixture for the same conditions as mentioned in previous section (i.e., applied voltage of 5 kV at a frequency of 10 kHz). Figure 13 illustrates the densities of the various molecules, plotted as a function of the initial O_2 fraction in the mixture, after a residence time of 5 s. This figure should be compared with Figure 9 above. Note, however, that the O_2 fraction is limited to 10–30%, to avoid the explosion regime, which occurs when the CH_4 fraction in pure O_2 reaches 61 mol%.[86]

In contrast to the CO_2/CH_4 mixture (Figure 9 above), the higher hydrocarbons are formed in somewhat lower amounts in the CH_4/O_2 mixture (see top panel of Figure 13), and different types of higher oxygenates become important, such as methanol (CH_3OH), methyl hydroperoxide (CH_3OOH), and ethyl hydroperoxide (C_2H_5OOH), while formaldehyde

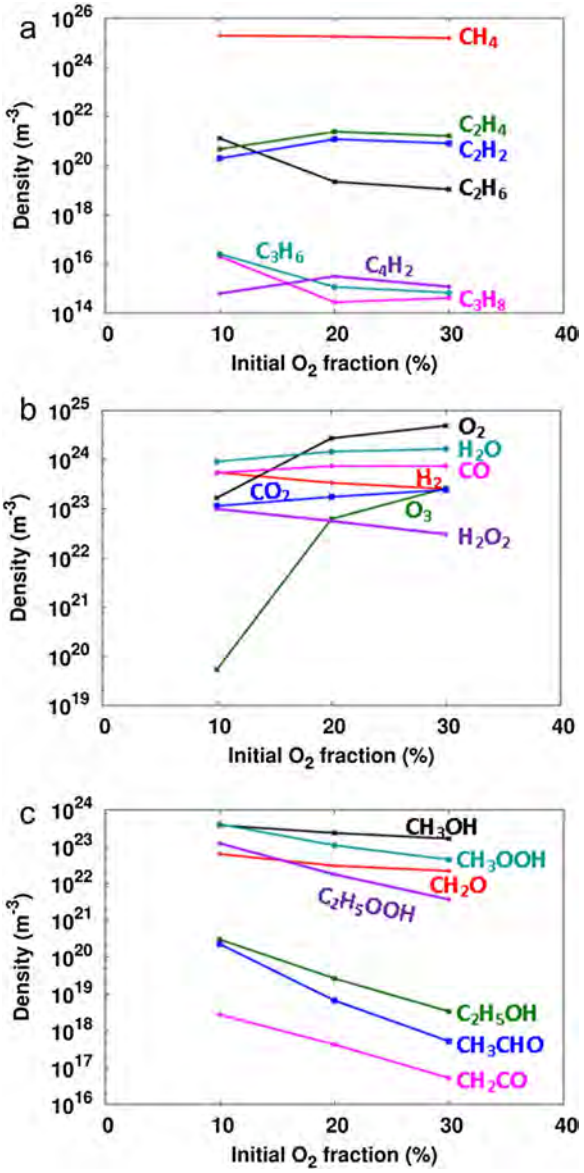

FIGURE 13 Calculated densities of CH_4 and O_2, as well as the various molecules formed in the CH_4/O_2 mixture, after a residence time of 5 s, as a function of O_2 fraction in the mixture, for a DBD reactor operating at 5 kV and 10 kHz

(CH_2O) is somewhat less important (see bottom panel of Figure 13). The same colors are used for the same products in Figures 9 and 13, to allow an easy comparison. Furthermore, some other major products are H_2O, CO, H_2, and unwanted CO_2, as well as H_2O_2 (decreasing upon higher O_2 fraction) and O_3 (increasing upon higher O_2 fraction); see middle panel of Figure 13. CO is now formed in larger amounts than H_2, yielding a H_2/CO ratio below 1, while it was above 1 in the CO_2/CH_4 mixture (see above). This illustrates that the H_2/CO ratio in the produced syngas can easily be varied, by altering the gas mixture and gas mixing ratio in a DBD, which might be less straightforward in classical processes, such as DRM (CO_2/CH_4), steam reforming (H_2O/CH_4) and partial oxidation of CH_4 (O_2/CH_4), which typically produce syngas with H_2/CO ratios below 1, above 3, and above 2, respectively.[87,88]

It is also clear from Figure 13 that the densities of the major oxygenates decrease over one (or more) order(s) of magnitude when the O_2 fraction in the mixture rises from 10 to 30%, while the densities of CO, CO_2, H_2O, and especially O_3 increase up to one order of magnitude (and more for O_3), pointing towards full oxidation of CH_4. Thus, if the production of specific oxygenates (like methanol) is targeted, our calculations predict that preferably not too high O_2 fractions should be used. This outcome, as well as more in general the calculated product formations illustrated in Figure 13, are in reasonable agreement with literature results, as explained in detail in.[62]

The conversion of CH_4, after this residence time of 5 s, is again calculated to be about 10%, like in the CO_2/CH_4 mixture (for the same CO_2 fraction up to 30%; see previous section). The O_2 conversion is calculated to be near 100% for 10% O_2 fraction in the mixture, which is attributed to three-body reactions of O_2 with CH_3 or H radicals. This conversion is much higher than the corresponding CO_2 conversion in the CO_2/CH_4 mixture (see previous section), illustrating the reactivity of O_2 towards the formation of many (partially or fully) oxygenated products. At higher O_2 fractions in the mixture, the O_2 conversion decreases, to about 35% at an O_2 fraction of 30%, because of the lower importance of the above process (see details in ref.[62]).

The calculated densities of the various molecules (plotted in Figure 13) also give information about their yields. The maximum yields of H_2, CO, formaldehyde, and methanol were found to be 9, 10, 0.3, and 4%, respectively. When comparing to the maximum yields for these products in the CO_2/CH_4 mixture (see previous section), it is clear that H_2 is formed in clearly less amounts (as also mentioned above), formaldehyde is also somewhat less important, but the methanol yield is one order of magnitude higher than the maximum yield in the CO_2/CH_4 mixture. The corresponding methanol selectivity was even calculated to be 15% (see[62] for details). This shows that the underlying chemistry in the CO_2/CH_4 and CH_4/O_2 mixtures is clearly different.

The latter is indeed clear from the reaction pathways illustrated in Figure 14, in comparison with Figure 10 above. Note that the thickness of the arrow lines is again correlated to the rate of the net reaction. Electron impact dissociation of CH_4 again leads to CH_3 radicals, which will recombine into methanol or higher hydrocarbons. More important, however, is the recombination into CH_3O_2 radicals, which form either CH_3O radicals or methyl hydroperoxide (CH_3OOH). The CH_3O radicals produce methanol, which appears a more important formation mechanism than the recombination of CH_3 with OH radicals (cf. the arrow line thickness in Figure 14). Methanol can also react further into CH_2OH radicals, which forms formaldehyde, and the latter is also easily converted into CHO radicals, and further into CO (note

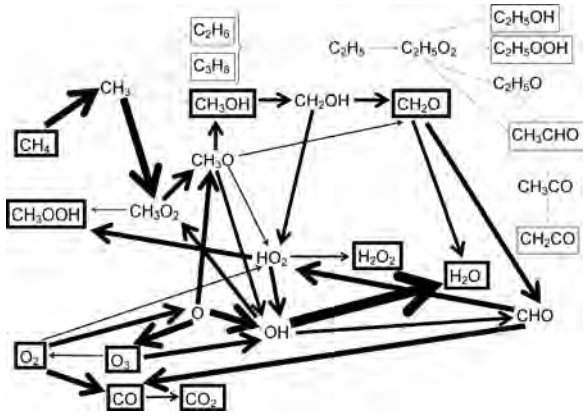

FIGURE 14 Schematic overview of the dominant reaction pathways for the conversion of CH_4 and O_2 into (mainly) higher oxygenates, as well as some full oxidation products, in a 70/30 CH_4/O_2 DBD plasma, operating at 5 kV and 10 kHz. The thickness of the arrow lines is correlated to the importance of the reaction paths

the thickness of these arrow lines, indicating the importance of these reactions) and CO_2. Furthermore, formaldehyde is also partially converted into H_2O.

It should be realized that this pathway is illustrated for the 70/30 CH_4/O_2 mixture, and it is clear that this mixing ratio leads to nearly full oxidation of CH_4, rather than partial oxidation, where the major end products should be the higher oxygenates. In the 90/10 CH_4/O_2 mixture, the situation is somewhat different, with methanol and methyl hydroperoxide formed in nearly equal amounts as CO and H_2O (see Figure 13 above).

As is also apparent from Figure 14, O_2 is mainly converted into CO, O atoms, and HO_2 radicals. Some O_3 is also formed out of O_2, but the reverse process, that is, the formation of two O_2 molecules out of O_3 and O atoms, is more important, explaining why the arrow points from O_3 towards O_2. The balance between O, O_2, and O_3 was also clear from Figure 2 above, and is explained in detail in ref.[12] The O atoms are also converted into CH_3O and OH radicals, leading further to methanol and water, respectively. Especially the latter reaction (from OH to H_2O) appears to be very important, as indicated from the thick arrow line, explaining why significant amounts of H_2O are formed, as illustrated in Figure 13 above. When comparing Figure 14 with Figure 10 above, it is clear that the chemical pathways in a CH_4/O_2 and CO_2/CH_4 plasma are quite different, even at the same mixing ratios, explaining why the product formation is also different.

4.5 | CO_2/H_2O mixture

The aim of studying the CO_2/H_2O plasma chemistry is to elucidate whether value-added chemicals, like methanol, can be more easily formed than in a CO_2/CH_4 mixture. Moreover, H_2O is a cheaper H-source, and the combined CO_2 and H_2O conversion could mimic the natural photosynthesis process.

Figure 15 illustrates the measured and calculated CO_2 and H_2O conversions, as well as the formed H_2/CO ratio, as a function of H_2O content in the gas mixture, at a CO_2 gas flow rate of 600 mL/min, and three different SEI values, as indicated in the legend. The experiments were carried out by

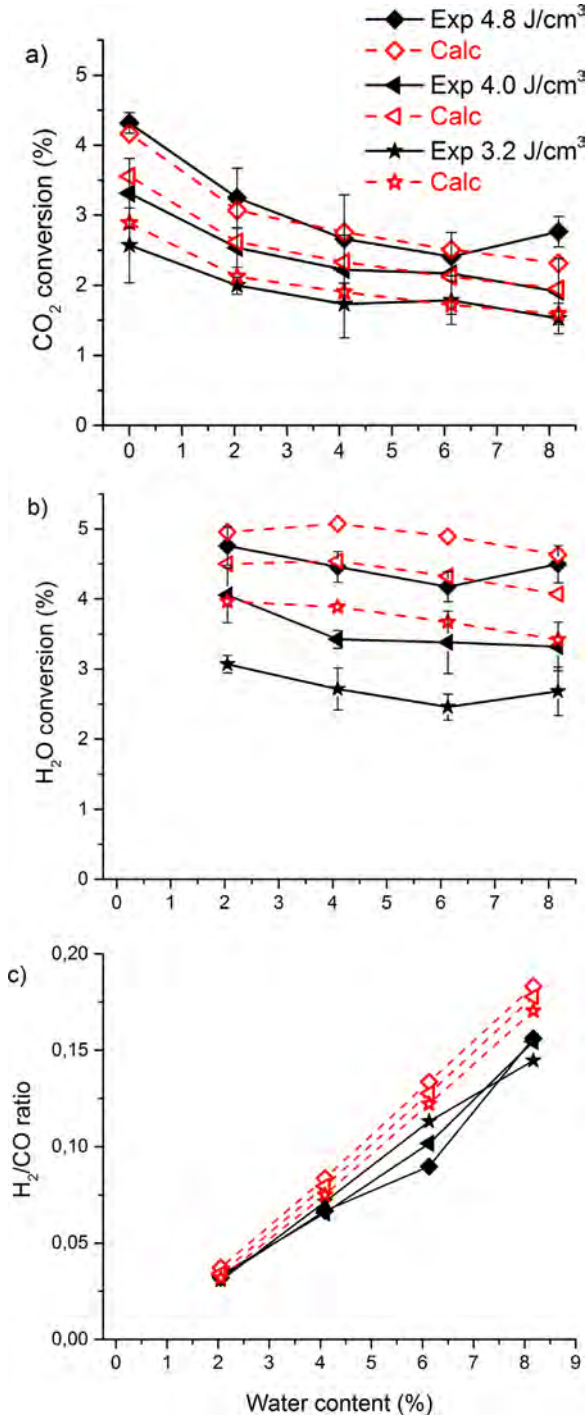

FIGURE 15 Calculated (dashed lines, open symbols) and measured (solid lines, filled symbols) CO_2 conversion (a), H_2O conversion (b), and formed H_2/CO ratio (c), in a DBD plasma, as a function of H_2O content in the gas mixture, at a total gas flow rate of 600 mL/min, and three different SEI values

Ozkan et al. (Université Libre de Bruxelles). The water vapor was generated in a controlled manner using a steam generator (CEM mixer Bronkhorst). Up to 8% water vapor was added to the CO_2 plasma. Furthermore, the entire system was heated to 50 °C to avoid condensation and to promote nebulization of the water through the discharge. More details about the experiments can be found in ref.[69]

The CO_2 conversion (Figure 15(a)) drops upon increasing H_2O content, at the three SEI values investigated, especially for low H_2O contents. This will be explained below. Very good agreement is reached between the calculated and measured values. The H_2O conversion (Figure 15(b)) also slightly drops upon higher H_2O content. The calculated H_2O conversions are slightly higher than the experimental values, that is, on average by about 10, 24, and 37%, for the SEI values of 4.8, 4.0, and 3.2 J/cm^3, respectively, in the entire range of water contents investigated. This might be due to some more complex processes taking place in the experiment, like condensation, which could not easily be account for in the 0D plasma chemistry model, as explained in ref.[69] At higher SEI, the probability of condensation is reduced, explaining the better agreement between the calculated and experimental H_2O conversions.

The main products formed by this conversion process are CO, H_2, O_2, and H_2O_2. No methanol was detected in the experiments and the calculated methanol concentrations are also not higher than the ppm level. The H_2/CO ratio (Figure 15(c)) is found to increase linearly with rising water content, from 0.03 at 2% water, to about 0.16 at 8% water content, both in the simulations and in the experiments. These ratios are rather low, but it is like expected, in view of the low H_2O fraction in the mixture. Higher H_2O fractions should give rise to correspondingly higher H_2/CO ratios. In general it is clear that the combined CO_2 and H_2O conversion allows for a process with an easily controlled syngas ratio, which is an important benefit, because several post-processes require a different syngas ratio, depending on the targeted product.[89]

Besides the CO_2 and H_2O conversion and the syngas ratio, also the calculated product selectivities are found in very good agreement with experimental data.[69] Thus, the model can be used to explain the observed trends and even steer the future experiments in a certain direction, to improve the desired product yields. A kinetic analysis of the reaction chemistry reveals that the reaction between CO and OH, yielding H atoms and CO_2, is crucial, as it has a very high rate constant, and it controls the ratio between the conversion of CO_2 and H_2O. This can be explained in a very simple way by the following reactions:

$$e^- + CO_2 \rightarrow CO + O + e^- \quad (1)$$

$$e^- + H_2O \rightarrow OH + H + e^- \quad (2)$$

$$CO + OH \rightarrow CO_2 + H \quad (3)$$

$$H + O_2 + M \rightarrow HO_2 + M \quad (4)$$

$$HO_2 + O \rightarrow OH + O_2 \quad (5)$$

$$OH + H \rightarrow H_2O \quad (6)$$

$$2e^- + CO_2 + H_2O \rightarrow CO_2 + H_2O + 2e^- \quad (7)$$

Reactions (1) and (2) lead to dissociation of CO_2 and H_2O, but the products, CO and OH, will rapidly recombine to form again CO_2 (reaction 3). Furthermore, the two H atoms and one O atom formed in this way, will also recombine quickly, first into OH (through the subsequent reactions (4) and (5)), and subsequently into H_2O through reaction (6). Thus, overall, there is no net dissociation of CO_2 and H_2O in this pathway (see overall reaction (7)).

Of course, this does not mean that there will be no net conversion of CO_2 and H_2O in the plasma, as there exist also other pathways for the conversion of these molecules. However, electron impact dissociation is typically the major loss mechanism for CO_2 in a DBD, as discussed above. Hence, the above mechanism explains the drop in CO_2 conversion upon addition of H_2O, as the OH radicals created from the dissociation of H_2O give rise to the backward reaction, creating CO_2 out of CO. This drop in absolute CO_2 conversion upon addition of H_2O is remarkable, because in general, we always observe a rise in absolute CO_2 conversion upon addition of another gas, such as N_2,[70–71] He[2,13] or Ar.[13]

Moreover, the above mechanism also explains why no methanol (or other oxygenated hydrocarbon) formation is observed in the CO_2/H_2O mixture. Indeed, all the H atoms needed to form CH and CHO fragments for the formation of methanol, seem to be steered to OH and subsequently H_2O again. Hence, this chemical analysis illustrates that H_2O might not be a suitable H-source for the formation of oxygenated hydrocarbons in a one-step process, because of the abundance of O atoms, O_2 molecules and OH radicals, trapping the H atoms. Note that this fast reaction between H and O atoms was demonstrated to be useful for the O-trapping in the case of pure CO_2 conversion, thus providing a solution for the separation of the CO_2 splitting products (see above), but in the present case, it is clearly the limiting factor for the formation of oxygenated hydrocarbons. In ref.[69] we have proposed some solutions on how the production of such oxygenated hydrocarbons could be targeted in a CO_2/H_2O plasma. One of the possibilities should be plasma catalysis. Specifically, we should look for a catalytic system that is able to recombine the H atoms into H_2, before they can recombine with O atoms into OH and H_2O, and that is also able to transform the CO together with H_2 into methanol before CO recombines with OH to CO_2. We believe there is quite some potential in plasma catalysis for this system, but a lot of research is still needed.

5 | CONCLUSIONS AND PERSPECTIVES FOR FUTURE WORK

This paper gives an overview of our plasma chemistry modeling work for CO_2 and CH_4 conversion in a DBD and a MW plasma, both in the pure gases and in various mixtures, that is, with each other and also with H_2O and O_2. To describe the detailed plasma chemistry, which lies at the basis of the conversion, a 0D chemical kinetics model or a 1D fluid model are the most appropriate. These models do not consider the detailed reactor geometry, but they can account for specific features, like the occurrence of microdischarge filaments in a DBD, by applying a large number of microdischarge pulses as a function of time in the 0D model, to mimic the filaments which the gas molecules can pass while travelling through the DBD reactor.

The models show that in a DBD the conversion is governed by electron impact dissociation (as well as ionization and/or electronic excitation) for the various gases investigated, while in a MW plasma, electron impact vibrational excitation of CO_2 is most important, due to the lower reduced electric field and thus the lower electron energies. The lower CO_2 vibrational levels produced in this way are gradually converted into the higher vibrational levels by vibrational-vibrational relaxation processes, that is, so-called ladder climbing, until they dissociate, mainly upon collision with O atoms or other heavy particles. As this process requires less energy than electron impact dissociation (or ionization or electronic excitation) from the CO_2 ground state, it can explain the higher energy efficiency obtained in a MW plasma compared to a DBD. Furthermore, it is also demonstrated that the energy efficiency of CO_2 splitting is higher at lower gas temperature, because of the reduced loss rates by vibrational-translational relaxation processes. Only at very high temperatures, when the vibrational population is thermal, the energy efficiency becomes comparable to the values at room temperature, but at these conditions the advantage of a non-equilibrium plasma for selective electron impact excitation to the CO_2 vibrational levels is lost. Besides the gas temperature, we have also discussed other major effects that may limit the energy efficiency, and we also propose solutions how to overcome these limitations.

In a DBD, the conversion typically rises with specific energy input for the various gases investigated, while the energy efficiency shows the opposite trend. Thus, there is a trade-off between conversion and energy efficiency, which is very clearly demonstrated for the CO_2/CH_4 mixture. For this gas mixture, we have also performed an extensive computational optimization study, based on 750 simulations, in a wide range of gas mixing ratios, power, residence time and frequency, to investigate which of these parameters yields the most promising results. After careful optimization of the operating conditions, an overall ($CO_2 + CH_4$) conversion up to 85% was predicted by the model, which is significantly higher than typical values obtained at more common operating conditions, reported in literature. This shows that there is still some room for improvement. However, the corresponding energy efficiency, even at the optimized conditions, is only in the order of 10%, and this is probably too low for industrial implementation. Indeed, for classical DRM, we estimated a maximum theoretical energy efficiency of 58%, so if the energy efficiency is the key performance indicator for this process, a DBD plasma might not be competitive with the classical DRM process. However, it also needs to be mentioned that the classical process might also not be able to reach this theoretical maximum, due to, e.g., thermal losses. Furthermore, we believe there is still room for improvement in the conversion and energy efficiency of a DBD plasma, by inserting dielectric beads, that is, in a packed bed DBD reactor.[10,14]

While CO_2 splitting mainly yields CO and O_2 formation, CH_4 reforming produces a variety of higher order hydrocarbons, besides H_2 gas. The same is true for the mixtures of CH_4 with CO_2 or O_2, where various higher hydrocarbons and oxygenates are formed. However, syngas (CO/H_2) is clearly the major product in CO_2/CH_4 or CH_4/O_2 conversion, and the yields and selectivities of the higher hydrocarbons and oxygenates are rather low. The same trends are also experimentally observed. Obviously, if specific value-added compounds (besides syngas) are targeted, the plasma will have to be combined with a suitable catalyst.

In contrast to the CO_2/CH_4 or CH_4/O_2 mixtures, the CO_2/H_2O mixture does not form many different oxygenates. Furthermore, the CO_2 conversion is reduced upon H_2O addition. Both observations are also made experimentally, and they can be explained from the model, by analyzing the chemical reaction pathways in the plasma. Indeed, our model predicts that the CO molecules, formed by CO_2 splitting, react with OH radicals, originating from H_2O splitting, back into CO_2, while the formed H and O atoms react back into H_2O, explaining the limited CO_2 and H_2O conversions. Furthermore, this explains why no oxygenates are formed, because all the H atoms, which would be needed to create these oxygenates, are trapped by the O atoms into the formation of OH and H_2O.

To validate our models, the computational results are compared as much as possible with experimental data, obtained either in our own group, or upon collaboration with other groups, or based on literature data. In general, a very good agreement is obtained, which allows us to use the models for obtaining a better understanding of the underlying plasma chemistry of CO_2 and CH_4 conversion and of the product formation, as explained above. This will be useful for further improving the performance of plasma technology for this application. For instance, the pathway analysis (for CO_2/CH_4 and CH_4/O_2) allows us to define the most suitable gas mixture (and mixing ratio) for obtaining the highest yields

or selectivities for the desired products. However, it is clear that the plasma chemistry is rather complicated and a lot of different molecules are formed. Therefore, as mentioned above, in order to selectively produce specific compounds, the combination with catalysis will be crucial.

Another example where the detailed insight in the underlying chemical reactions can provide possible solutions on how to improve the performance of the conversion was illustrated for the problem of CO/O_2 product separation in pure CO_2 splitting. Indeed, it was found that by adding a few % of a H-source, such as H_2 or CH_4, all the O atoms formed by CO_2 splitting can react with H atoms to form H_2O instead of O_2 gas, and the H_2O can be more easily separated from the gas mixture. This chemical trapping can also be useful for enhancing the CO_2 conversion according to Le Chatelier's law, by removing the O_2 from the plasma.

The results presented here are all obtained with a 0D chemical kinetics model or a 1D fluid model, which is indeed most convenient for describing the detailed plasma chemistry. However, in order to account for details in the reactor configuration, and to predict how modifications to the reactor geometry yield better CO_2 conversion and energy efficiency, two-dimensional and three-dimensional models will be required. Within our group, we are working on such models for a packed bed DBD reactor,[90] MW plasma and GA reactor.[91–93] However, because of the much higher computational cost of such two-dimensional or three-dimensional models, they are in first instance developed for argon or helium gas, because of the more simple reaction chemistry, which is needed to limit the calculation time. Nevertheless, in the future, we plan to extend these models to CO_2 (and its mixtures), in order to model the CO_2 conversion in a real plasma reactor geometry. For this purpose, the plasma chemistry will have to be reduced, as demonstrated for CO_2 splitting in[12,46] for typical DBD and MW plasma conditions, respectively.

Furthermore, to describe the CO_2/CH_4 or CO_2/H_2O conversion in a MW plasma or GA reactor, we will also need to include the vibrational levels of CH_4 and H_2O, as the latter might play a significant role in this type of plasmas for determining the energy efficiency, as was demonstrated in this paper for pure CO_2 splitting. However, describing the vibrational kinetics of CH_4 and H_2O is a non-trivial task, because of the many vibrational modes of these molecules. A detailed description of the latter cannot be included in a two-dimensional or three-dimensional model, but should be performed again in a 0D model.

Another possible improvement of our 0D model would be to focus explicitly on the calculation of the electron energy distribution function (EEDF), to understand its dependence on the presence of electronically and vibrationally excited states of CO_2. This was also recently thoroughly investigated by Pietanza et al.[94–97] studying the free electron kinetics in CO_2 plasma.

Finally, to better understand the underlying mechanisms of plasma catalysis, we are also studying the behavior of plasma inside catalyst pores,[98] as well as the chemical interactions between plasma species and a catalyst material by means of atomic scale simulations.[99–101] However, still a lot of work will be needed before we can provide the necessary insights into the most suitable catalyst material, and how to steer the process towards the production of specific components.

ACKNOWLEDGMENTS

We would like to thank B. Verheyde and S. Paulussen (VITO), X. Tu and coworkers (University of Liverpool), A. Ozkan, Th. Dufour, and F. Reniers (Université Libre de Bruxelles), for providing some experimental data to validate our models, as well as M. Kushner (University of Michigan) and J. van Dijk (Eindhoven University of Technology) for providing some of the models using in this work, and R. Aerts for generating some of the modeling results. Furthermore, we acknowledge financial support from the IAP/7 (Inter-university Attraction Pole) program 'PSI-Physical Chemistry of Plasma-Surface Interactions' by the Belgian Federal Office for Science Policy (BELSPO), the Francqui Research Foundation, the Fund for Scientific Research Flanders (FWO; Grant no. G.0383.16N). The calculations were carried out using the Turing HPC infrastructure at the CalcUA core facility of the Universiteit Antwerpen (UAntwerpen), a division of the Flemish Supercomputer Center VSC, funded by the Hercules Foundation, the Flemish Government (department EWI) and the UAntwerpen.

REFERENCES

[1] S. Paulussen, B. Verheyde, X. Tu, C. De Bie, T. Martens, D. Petrovic, A. Bogaerts, B. Sels, *Plasma Sources Sci. Technol.* **2010**, *19*, 034015.

[2] N. R. Pinhao, A. Janeco, J. B. Branco, *Plasma Chem Plasma Proc.* **2011**, *31*, 427.

[3] B. Eliasson, U. Kogelschatz, B. Xue, L.-M. Zhou, *Ind. Eng. Chem. Res.* **1998**, *37*, 3350.

[4] Q. Wang, Y. Cheng, Y. Jin, *Catal. Today* **2009**, *148*, 275.

[5] A.-J. Zhang, A-M. Zhu, J. Guo, Y. Xu, C. Shi, *Chem Eng. J.* **2010**, *156*, 601.

[6] X. Tu, H. J. Gallon, M. V. Twigg, P. A. Gorry, J. C. Whitehead, *J. Phys. D: Appl. Phys.* **2011**, *44*, 274007.

[7] T. Nozaki, K. Okazaki, *Catal. Today* **2013**, *211*, 29.

[8] A. Gómez-Ramírez, V. J. Rico, J. Cotrino, A. R. González-Elipe, R. M. Lambert, *ACS Catal.* **2014**, *4*, 402.

[9] M. Scapinello, L. M. Martini, P. Tosi, *Plasma Proc. Polym.* **2014**, *11*, 624.

[10] D. Mei, X. Zhu, Y. He, J. D. Yan, X. Tu, *Plasma Sources Sci. Technol.* **2015**, *24*, 015011.

[11] A. Ozkan, T. Dufour, G. Arnoult, P. De Keyzer, A. Bogaerts, F. Reniers, *J. CO_2 Util.* **2015**, *9*, 74.

[12] R. Aerts, W. Somers, A. Bogaerts, *ChemSusChem*. **2015**, *8*, 702.

[13] M. Ramakers, I. Michielsen, R. Aerts, V. Meynen, A. Bogaerts, *Plasma Process. Polym*. **2015**, *12*, 755.

[14] K. Van Laer, A. Bogaerts, *Energy Technol*. **2015**, *3*, 1038.

[15] R. I. Asisov, V. K. Givotov, E. G. Krasheninnikov, B. V. Potapkin, V. D. Rusanov, A. Fridman, *Sov. Phys. Doklady* **1983**, *271*, 94.

[16] L. F. Spencer, A. D. Gallimore, *Plasma Sources Sci. Technol*. **2013**, *22*, 015019.

[17] T. Silva, N. Britun, T. Godfroid, R. Snyders, *Plasma Sources Sci. Technol*. **2014**, *23*, 025009.

[18] A. P. H. Goede, W. A. Bongers, M. F. Graswinckel, M. C. M. van de Sanden, M. Leins, J. Kopecki, A. Schulz, M. Walker, EPJ Web of Conferences, 3rd Eur. Energy Conference, **2013**.

[19] W. A. Bongers, S. Welzel, D. C. M. van den Bekerom, G. Frissen, G. J. van Rooij, A. P. H. Goede, M. F. Graswinckel, P. Groen, N. den Harder, B. van Heemert, T. Minea, M. C. M. van de Sanden, M. Leins, J. Kopecki, A. Schulz, M. Walker, Proceedings 22nd International Symposium on Plasma Chemistry (Antwerp, Belgium), **2015**.

[20] G. J. van Rooij, D. C. M. van den Bekerom, N. den Harder, T. Minea, G. Berden, W. A. Bongers, R. Engeln, M. F. Graswinckel, E. Zoethout, M. C. M. van de Sanden, *Faraday Discuss*. **2015**, *183*, 233.

[21] M. Scapinello, L. M. Martini, G. Dilecce, P. Tosi, *J. Phys. D: Appl. Phys*. **2016**, *49*, 075602.

[22] X. S. Li, B. Zhu, C. Shi, Y. Xu, A. M. Zhu, *AIChE J*. **2011**, *57*, 2854.

[23] B. Zhu, X. S. Li, C. Shi, J. L. Liu, T. L. Zhao, A. M. Zhu, *Int. J. Hydrogen Energy* **2012**, *37*, 4945.

[24] B. Zhu, X. S. Li, J. L. Liu, X. Zhu, A. M. Zhu, *Chem. Eng. J*. **2015**, *264*, 445.

[25] C. S. Kalra, Y. I. Cho, A. Gutsol, A. Fridman, T. S. Rufael, *Rev. Sci. Instrum*. **2005**, *76*, 025110.

[26] A. Indarto, D. R. Yang, J.-W. Choi, H. Lee, H. K. Song, *J. Hazard. Mater*. **2007**, *146*, 309.

[27] T. Nunnally, K. Gutsol, A. Rabinovich, A. Fridman, A. Gutsol, A. Kemoun, *J. Phys. D. Appl. Phys*. **2011**, *44*, 274009.

[28] H. Lee, H. Sekiguchi, *J. Phys D: Appl. Phys*. **2011**, *44*, 274008.

[29] X. Tu, J. C. Whitehead, *Int. J. Hydrogen Energy* **2014**, *39*, 9658.

[30] J. L. Liu, H. W. Park, W. J. Chung, D. W. Park, *Chem. Eng. J*. **2016**, *285*, 234.

[31] J. L. Liu, H. W. Park, W. J. Chung, D. W. Park, *Plasma Chem. Plasma Process*. **2016**, *36*, 437.

[32] K. Li, J. L. Liu, X. S. Li, X. Zhu, A. M. Zhu, *Chem. Eng. J*. **2016**, *288*, 671.

[33] H. L. Chen, H. M. Lee, S. H. Chen, Y. Chao, M. B. Chang, *Appl. Catal. B: Environ*. **2008**, *85*, 1.

[34] E. C. Neyts, K. Ostrikov, M. K. Sunkara, A. Bogaerts, *Chem. Rev*. **2015**, *115*, 13408.

[35] A. Cenian, A. Chernukho, V. Borodin, G. Sliwinski, *Contrib. Plasma Phys*. **1994**, *34*, 25.

[36] A. Cenian, A. Chernukho, V. Borodin, *Contrib. Plasma Phys*. **1995**, *35*, 273.

[37] H. Hokazono, H. Fujimoto, *J. Appl. Phys*. **1987**, *62*, 1585.

[38] A. Fridman, *Plasma Chemistry*. Cambridge University Press, Cambridge **2008**.

[39] B. F. Gordiets, A. I. Osipov, E. V. Stupochenko, L. A. Shelepin, *Soviet Physics Uspekhi* **1973**, *15*, 759.

[40] E. Kustova, E. Nagnibeda, *Chem. Phys*. **2006**, *321*, 293.

[41] V. D. Rusanov, A. A. Fridman, G. V. Sholin, *Soviet Physics Uspekhi* **1981**, *24*, 447.

[42] R. Aerts, T. Martens, A. Bogaerts, *J. Phys. Chem. C* **2012**, *116*, 23257.

[43] T. Kozák, A. Bogaerts, *Plasma Sources Sci. Technol*. **2014**, *23*, 045004.

[44] T. Kozák, A. Bogaerts, *Plasma Sources Sci. Technol*. **2015**, *24*, 015024.

[45] S. Ponduri, M. M. Becker, S. Welzel, M. C. M. van de Sanden, D. Loffhagen, R. Engeln, *J. Appl. Phys*. **2016**, *119*, 093301.

[46] A. Berthelot, A. Bogaerts, *Plasma Sources Sci. Technol*. **2016**, *25*, 045022.

[47] Y. Yang, *Plasma Chem. Plasma Process*. **2003**, *23*, 327.

[48] A. Indarto, N. Coowanitwong, J.-W. Choi, H. Lee, H. K. Song, *Fuel Process. Technol*. **2008**, *89*, 214.

[49] C. De Bie, B. Verheyde, T. Martens, J. van Dijk, S. Paulussen, A. Bogaerts, *Plasma Process. Polym*. **2011**, *8*, 1033.

[50] J. Luche, O. Aubry, A. Khacef, J. M. Cormier, *Chem. Eng. J*. **2009**, *149*, 35.

[51] L. M. Zhou, B. Xue, U. Kogelschatz, B. Eliasson, *Energ. Fuel*. **1998**, *12*, 1191.

[52] H. Machrafi, S. Cavadias, J. Amouroux, *J. Phys.: Conf. Ser*. **2011**, *275*, 012016.

[53] V. Goujard, J. M. Tatibouet, C. Batiot-Dupeyrat, *Plasma Chem. Plasma Process*. **2011**, *31*, 315.

[54] J. G. Wang, C. J. Liu, B. Eliasson, *Energ. Fuel*. **2004**, *18*, 148.

[55] I. Istadi, N. A. S. Amin, *Chem. Eng. Sci*. **2007**, *62*, 6568.

[56] M. Kraus, W. Egli, K. Haffner, B. Eliasson, U. Kogelschatz, A. Wokaun, *Phys. Chem. Chem. Phys*. **2002**, *4*, 668.

[57] C. J. Liu, Y. Li, Y. P. Zhang, Y. Wang, J. Zou, B. Eliasson, B. Xue, *Chem. Lett*. **2001**, *12*, 1304.

[58] C. De Bie, T. Martens, J. van Dijk, S. Paulussen, B. Verheyde, A. Bogaerts, *Plasma Sources Sci. Technol*. **2011**, *20*, 024008.

[59] R. Snoeckx, R. Aerts, X. Tu, A. Bogaerts, *J. Phys. Chem. C* **2013**, *117*, 4957.

[60] R. Snoeckx, Y. X. Zeng, X. Tu, A. Bogaerts, *RSC Adv*. **2015**, *5*, 29799.

[61] A. Janeco, N. R. Pinhão, V. Guerra, *J. Phys. Chem. C* **2015**, *119*, 109.

[62] C. De Bie, J. van Dijk, A. Bogaerts, *J. Phys. Chem. C* **2015**, *119*, 22331.

[63] L. M. Zhou, B. Xue, U. Kogelschatz, B. Eliasson, *Plasma Chem. Plasma Process*. **1998**, *18*, 375.

[64] S. A. Nair, T. Nozaki, K. Okazaki, *Chem. Eng. J.* **2007**, *132*, 85.

[65] V. Goujard, T. Nozaki, S. Yuzawa, A. Ağiral, K. Okazaki, *K. J. Phys. D: Appl. Phys.* **2011**, *44*, 274011.

[66] A. Agiral, T. Nozaki, M. Nakase, S. Yuzawa, K. Okazaki, J. G. E. Gardeniers, *Chem. Eng. J.* **2011**, *167*, 560.

[67] J. Zhou, Y. Xu, X. Zhou, J. Gong, Y. Yin, H. Zheng, H. Guo, *ChemSusChem* **2011**, *4*, 1095.

[68] N. S. Matin, J. C. Whitehead, 28th ICPIG, July 15–20, 2007, Prague, Czech Republic **2007**, 983.

[69] R. Snoeckx, A. Ozkan, F. Reniers, A. Bogaerts, (in preparation).

[70] S. Heijkers, R. Snoeckx, T. Kozák, T. Silva, T. Godfroid, N. Britun, R. Snyders, A. Bogaerts, *J. Phys. Chem. C* **2015**, *119*, 12815.

[71] R. Snoeckx, S. Heijkers, K. Van Wesenbeeck, S. Lenaerts, A. Bogaerts, *Energy & Environm. Sci.* **2016**, *9*, 999.

[72] J. Legrand, A. Diamy, R. Hrach, V. Hrachova, *Vacuum* **1997**, *48*, 671.

[73] A. Majumdar, J. F. Behnke, R. Hippler, K. Matyash, R. Schneider, *J. Phys. Chem. A* **2005**, *109*, 9371.

[74] C. D. Pintassiglio, C. Jaoul, J. Loureiro, T. Belmonte, T. Czerwiec, *J. Phys. D: Appl. Phys.* **2007**, *40*, 3620.

[75] J. L. Jauberteau, I. Jauberteau, M. J. Cinelli, J. Aubreton, *New J. Phys.* **2002**, *4*, 1.

[76] S. Y. Savinov, H. Lee, H. Keun, B. Na, *Plasma Chem. Plasma Process.* **2003**, *23*, 159.

[77] R. Snoeckx, M. Setareh, R. Aerts, P. Simon, A. Maghari, A. Bogaerts, *Int. J. Hydrogen Energy* **2013**, *38*, 16098.

[78] J. van Dijk, K. Peerenboom, M. Jimenez, D. Mihailova, J. van der Mullen, *J. Phys. D: Appl. Phys* **2009**, *42*, 194012.

[79] http://plasimo.phys.tue.nl.

[80] A. Bogaerts, W. Wang, A. Berthelot, V. Guerra, *Plasma Sources Sci. Technol.* **2016**, *25*, 055016.

[81] A. Bogaerts, T. Kozák, K. Van Laer, R. Snoeckx, *Faraday Discuss.* **2015**, *183*, 217.

[82] V. Givotov, A. Fridman, M. Krotov, E. Krasheninnikov, B. Patrushev, V. Rusanov, G. Sholin, *Int. J. Hydrogen Energy* **1981**, *6*, 441.

[83] R. Aerts, R. Snoeckx, A. Bogaerts, *Plasma Process. Polym.* **2014**, *11*, 985.

[84] A. Brunetti, F. Scura, G. Barbieri, E. Drioli, *J. Membr. Sci.* **2010**, *359*, 115.

[85] Y. Tagawa, S. Mori, M. Suzuki, I. Yamanaka, T. Obara, J. Ryu, Y. Kato, *Kagaku Kogaku Ronbun.* **2011**, *37*, 114.

[86] S. A. Lawton, A. V. Phelps, *J. Chem. Phys.* **1978**, *69*, 1055.

[87] L. M. Zhou, B. Xue, U. Kogelschatz, B. Eliasson, *Energ. Fuel.* **1998**, *12*, 1191.

[88] K. Zhang, U. Kogelschatz, B. Eliasson, *Energ. Fuel.* **2001**, *15*, 395.

[89] P. L. Spath, D. C. Dayton, *Report Natl. Renew. Energy Lab.* **2003**, 1.

[90] K. Van Laer, A. Bogaerts, *Plasma Sources Sci. Technol.* **2016**, *25*, 015002.

[91] St. Kolev, A. Bogaerts, *Plasma Sources Sci. Technol.* **2015**, *24*, 015025.

[92] St. Kolev, A. Bogaerts, *Plasma Sources Sci. Technol.* **2015**, *24*, 065023.

[93] G. Trenchev, St. Kolev, A. Bogaerts, *Plasma Sources Sci. Technol.* **2016**, *25*, 035014.

[94] L. D. Pietanza, G. Colonna, G. D'Ammando, A. Laricchiuta, M. Capitelli, *Plasma Sources Sci. Technol. (Fast Track Commun.)* **2015**, *24*, 042002.

[95] L. D. Pietanza, G. Colonna, G. D'Ammando, A. Laricchiuta, M. Capitelli, *Chem. Phys.* **2016**, *468*, 44.

[96] L. D. Pietanza, G. Colonna, G. D'Ammando, A. Laricchiuta, M. Capitelli, *Phys. Plasmas* **2016**, *23*, 013515.

[97] L. D. Pietanza, G. Colonna, V. Laporta, R. Celiberto, G. D'Ammando, A. Laricchiuta, M. Capitelli, *J. Phys. Chem A* **2016**, *120*, 2614.

[98] Y.-R. Zhang, K. Van Laer, E. C. Neyts, A. Bogaerts, *Appl. Cat. B: Environ.* **2016**, *185*, 56.

[99] W. Somers, A. Bogaerts, A. C. T. van Duin, E. C. Neyts, *J. Phys. Chem. C* **2012**, *116*, 20958.

[100] W. Somers, A. Bogaerts, A. C. T. van Duin, S. Huygh, K. M. Bal, E. C. Neyts, *Catal. Today* **2013**, *211*, 131.

[101] W. Somers, A. Bogaerts, A. C. T. van Duin, E. C. Neyts, *Appl. Cat. B: Envir.* **2014**, *154–155*, 1.

AUTHORS' BIOGRAPHIES

A. Bogaerts was born in 1971. She obtained her PhD degree in Chemistry in 1996, from the University of Antwerp in Belgium. After some postdoc years, she became a professor of physical chemistry in 2003, at the same university, and is full professor since 2012. She is head of the interdisciplinary research group PLASMANT. Her research activities include the study of plasma chemistry, plasma reactor design, and plasma-surface interactions, mainly for environmental and medical applications, both by modeling and experiments. In recent years, special attention is given to CO_2 conversion by plasma and plasma catalysis.

C. De Bie was born in 1983. He received his master's degree in Chemistry in 2006 and his master's degree in Environmental Science in 2007 from the University of Antwerp in Belgium. Currently, he is affiliated as a PhD student to the research group PLASMANT at the same university. His research activities include the fluid modeling of dielectric barrier discharges for plasma-assisted conversion of greenhouse gases to value-added chemicals. Since 2012, he is also the president of The Royal Flemish Chemical Society.

R. Snoeckx was born in 1988. He obtained a master's degree in both Environmental Science (2010) and Chemistry (2012) from the University of Antwerp, and is currently finalising his PhD. Combining these two backgrounds he started his PhD work in chemistry at the research group PLASMANT on the topic of plasma based conversion of greenhouse gases into value-added chemicals and fuels. For this research he actively collaborated with several (inter) national research institutions, for example during research visits at the Instituto Superior Técnico, the King Abdullah University of Science and Technology, and the Drexel Plasma Institute.

T. Kozák was born in Klatovy (Czech Republic) in 1983. He received his master's and PhD degrees in Applied Physics from the University of West Bohemia in Plzeň (Czech Republic) in 2008 and 2013, respectively. In 2013 and 2014, he was working as a postdoctoral researcher in the PLASMANT research group at the University of Antwerp, focusing on the modelling of CO_2 splitting in plasmas. Currently, he is a junior researcher at the Research Center NTIS at the University of West Bohemia. His main interests are modeling of low-temperature non-equilibrium plasmas for thin film deposition, plasma chemistry, and plasma diagnostics.

How to cite this article: Bogaerts A, De Bie C, Snoeckx R, Kozák T. Plasma based CO_2 and CH_4 conversion: A modeling perspective. *Plasma Process Polym.* 2017;14:e1600070. https://doi.org/10.1002/ppap.201600070